Climate-Driven Projections of Future Global Wetlands Extent

Lucas Hardouin, Bertrand Decharme, Jeanne Colin, Christine Delire

Earth's Future

RESEARCH ARTICLE
10.1029/2024EF004553

Climate-Driven Projections of Future Global Wetlands Extent

Lucas Hardouin[1], **Bertrand Decharme**[1], **Jeanne Colin**[1], **and Christine Delire**[1]

[1]CNRM, Météo-France, CNRS, Université de Toulouse, Toulouse, France

Key Points:

- Projections of climate-driven changes in wetlands extent are analyzed using the sixth phase of the Coupled Model Intercomparison Project
- Consistent decrease in wetlands extent are projected over the Mediterranean, Central America, and Amazon Basin in South America
- There is significant uncertainty among models in high latitudes, but a subsample of models indicate a decrease in boreal wetlands extent

Supporting Information:

Supporting Information may be found in the online version of this article.

Correspondence to:

L. Hardouin,
lucas.hardouin@univ-tlse3.fr

Citation:

Hardouin, L., Decharme, B., Colin, J., & Delire, C. (2024). Climate-driven projections of future global wetlands extent. *Earth's Future*, *12*, e2024EF004553. https://doi.org/10.1029/2024EF004553

Received 16 FEB 2024
Accepted 12 AUG 2024

Abstract Wetlands are crucial components of the Earth's system, interacting with various processes such as the hydrological cycle, energy exchanges with the atmosphere, and global nitrogen and carbon cycles. The future trajectory of wetlands is anticipated to be influenced not only by direct human activities, but also by climate change. Here we present our assessment of climate-driven global changes in wetlands extent, focusing on the main wetland complexes. We used an approach based on the Topographic Hydrological model (TOPMODEL) and soil liquid water content projections from 14 models of the Coupled Model Intercomparison Project Phase 6 (CMIP6). Our analysis reveals a consistent decrease in wetlands extent in the Mediterranean, Central America, and northern South America, with a substantial loss of 28% in the western Amazon Basin for the end of the 21st century (2081–2100) under the SSP370 scenario. Conversely, Central Africa exhibits an increase in wetlands extent, except in the Congo Basin. Nevertheless, most of the areas studied (80%) present uncertain results, due to conflicting projections of changes between the models. Notably, we show that there is significant uncertainty among CMIP6 models regarding liquid soil water content in high latitudes. By narrowing our focus to 10 models, which seem to better represent the thawing of permafrost, we obtain a better inter-model agreement. We then find a modest declines in the overall global area (<5%), but an average loss of 13% beyond 50°N. Specific areas like the Hudson Bay Lowlands experiencing a 21% decrease and the Western Siberian Lowlands a 15% decrease.

Plain Language Summary Wetlands are vital ecosystems, that exchange matter and energy with other components of the Earth's system. They are expected to face changes in their functioning and extent due to both human activities and climate change. Our assessment using advanced models reveals consistent shrinking of wetlands extent in the Mediterranean, Central America, and parts of South America, with a significant loss projected in the western Amazon Basin. Conversely, Central Africa may see an increase, except in the Congo Basin. However, much of our findings carry uncertainty due to conflicting model projections, particularly regarding soil water content in high latitudes. Focusing on models better representing permafrost thawing, we find a modest global decline in wetland area, with notable decreases in specific regions like the Hudson Bay and Western Siberian Lowlands.

1. Introduction

Over the last few centuries of human history, wetlands were considered, especially by Western countries, as sources of disease, unsuitable for agriculture and settlement. They have therefore been dried out and converted to other land uses. Wetlands loss resulting directly from human activities since 1900 has been estimated at around 50% in the literature (ex (Zedler & Kercher, 2005)). Compiling scientific reports, Davidson (2014) points out great uncertainties in this estimation of the overall loss of wetland, due to the temporal and spatial heterogeneity of the records. The greatest losses occurred in Europe and North America, and the rate of loss has increased more rapidly in Asia and tropical regions over the 20th and 21st centuries. The recent study of Fluet-Chouinard et al. (2023) lowers the global estimates to 21% wetland loss since 1700. It highlights the spatially unequal nature of these losses and shows that previous studies are probably biased by the larger losses observed in Europe, North America, China and South–East Asia, while northern Canada and Siberia have been very little altered, and wetlands in South America and Central Africa are facing more recent threats (Dargie et al., 2019; Ikeda-Castrillon et al., 2020; Roucoux et al., 2017). As humankind has come to understand the critical ecosystem services wetlands were providing, conservation and management policies have developed. In 1971, it led to the Ramsar Convention, an international treaty aiming at maintaining the "ecological character" of all wetlands through "wise use" (Gardner & Finlayson, 2018). However, most natural wetlands are still shrinking at the global scale (Davidson &

Finlayson, 2018; Davidson et al., 2018). Their future trajectories will be driven by direct human activities, as well as pollution and climate change.

Wetlands interact with the rest of the Earth System through different processes involving the hydrological cycle (Bullock & Acreman, 2003), energy and water exchanges with the atmosphere (Decharme & Douville, 2007; Gedney & Cox, 2003; Krinner, 2003; Sterling et al., 2013), the global nitrogen cycle (Saunders & Kalff, 2001), and the global carbon cycle (Harenda et al., 2018; Mitra et al., 2005). The storage and fluxes of water, nitrogen and carbon related to wetlands all increase with their extent (Keddy et al., 2009). Wetland are the most important natural source of methane for the atmosphere (Saunois et al., 2020), a greenhouse gas much more powerful than CO_2 (Masson-Delmotte et al., 2021). The annual contribution of wetlands to global methane emissions varies between 20% and 30% (Kirschke et al., 2013; Saunois et al., 2020), and is highly dependent on climate variability. This contribution in the global budget is suspected to increase with climate change: changes recently observed in the growth rate of atmospheric methane concentration in 2020 and 2021 have been partially attributed to an increase of emissions from wetlands (Peng et al., 2022). This has been confirmed by an observed intensification of the methane-climate feedback (Zhang et al., 2023). However, the wetland methane-climate feedback remains poorly understood and uncertain (Dean et al., 2018), as changes in temperature and hydrological conditions can have indirect and compensatory effects on the processes that cause methane emissions (Walter & Heimann, 2000). For instance, the temperature rising enhances methanogenesis by accelerating the microbial activity and the carbon decomposition (Bardgett et al., 2008; Winden et al., 2012; Yvon-Durocher et al., 2014). At the same time, it can increase periods of drought, which lowers the water table and reduces CH_4 emissions (Huang et al., 2021; Mitsch et al., 2010; Olefeldt et al., 2017), while having an impact on the spatial and temporal extent of wetlands. In any case, changes in wetlands areas play an important role in inter-annual variations of CH_4 emissions (Ringeval et al., 2010). Taking into account their evolution with climate change is thus necessary to constrain part of the methane feedback (Bousquet et al., 2011; Bridgham et al., 2013; Kirschke et al., 2013).

Wetland definitions can vary among scientific communities. For the purpose of this study, we define wetlands as areas where the soil remains saturated with water for extended periods, providing a habitat conducive to vegetation adapted to saturated soil conditions. According to this definition, the wetlands extent in a given region is strongly related to the variations of soil moisture contents, which are themselves mostly driven by precipitation and evapotranspiration. Ice melting can also increase temporarily liquid water contents and alter the drainage efficiency at high latitudes (Kreplin et al., 2021; Woo & Young, 2006). These water fluxes and their temporal evolution can be simulated with Global Climate Models (GCMs), which also simulate soil water contents in their surface component, hereafter referred to as Land Surface Models (LSMs). However, their rather coarse resolution does not allow them to directly represent the wetland fraction in each grid cell. Over the past decade, an original way to represent wetlands in LSMs has been used by adapting the simple hydrological model TOPMODEL (Beven & Kirkby, 1979), generally used to simulate sub-grid hydrology in LSMs (Clark & Gedney, 2008; Decharme & Douville, 2006; Famiglietti & Wood, 1994; Gedney & Cox, 2003; Habets & Saulnier, 2001; Koster et al., 2000; Niu et al., 2005; Stieglitz et al., 1997). It is based on a statistical approach of the topography to predict the lateral distribution of water in a catchment. It uses a topographic index λ that determines the capacity of a pixel to be flooded, which is as a function of the local hydraulic gradient and the upstream drainage area. Most TOPMODEL implementations for wetland representation have been integrated directly into LSMs (Kleinen et al., 2012; Ringeval et al., 2012; Stocker et al., 2014; Zhang et al., 2016), but usually with no feedback on the soil water content, which means that simulations can also be carried out in "offline" mode by using soil moisture products (as in Xi et al., 2021, 2022; B. Zhao and Zhuang (2023)). The use of a uniform parameterization of TOPMODEL gave satisfactory results in the zonal representation of wetlands (Ringeval et al., 2012; Stocker et al., 2014), but with a slight global overestimation and strong local discrepancies compared to most of the observational surveys (Lehner & Döll, 2004; Schroeder et al., 2015; Zhang et al., 2021a). The study of Zhang et al. (2016) showed that the spatial distribution of wetlands can be considerably improved by a parameterization of TOPMODEL with grid points calibrated to a reference data set. It also highlights the importance of the resolution of Digital Elevation Models (DEMs) to calculate the topographic index. While TOPMODEL has been widely used to represent the spatio-temporal dynamics of wetlands worldwide over the historical period, only the study by Xi et al. (2021) refers to the impact of climate change on wetlands extent and it focuses on inland Ramsar sites. Their future projections are based on global climate models outputs of soil moisture, taken from climate change scenarios run for the Climate Model Intecomparisons Project Phase 5 (CMIP5) (Taylor et al., 2012). The

large uncertainties between model estimates led them to apply a correction factor derived from the GLDAS-Noah v2.0 reanalysis product (Rodell et al., 2004).

In this study, we develop a TOPMODEL-based approach to diagnose the wetlands extent in each grid cell of Global Climate Models (GCMs). It uses the corrected equations from Saulnier and Datin (2004) already used in Habets and Saulnier (2001), Decharme et al. (2006) and Ringeval et al. (2012) and introduces a local parameterization calibrated on recent observations of wetland areas. With this approach, we perform a multi-model analysis of the impact of climate change on wetlands extent at the global scale, using the generation of global climate models and greenhouse gas concentration scenarios which were used for CMIP6 (Sixth Coupled Model Intercomparison Project) (Eyring et al., 2016). Our method, detailed in Section 2, is applied to soil moisture outputs from CMIP6 simulations, run with 14 different models, over the historical (1850–2014) and future (2015–2100) periods, following four different scenarios for the 2015–2100 period. Results are analyzed in Section 3. We first consider the impact of calibration on our method, then the evolution of wetlands extent at the global scale, and finally we focus on the evolution of five major wetland complexes: the Amazon Basin, the Congo Basin, the Pantanal, the Hudson Bay Lowlands (HBL) and the Western Siberian Lowlands (WSL). In Section 4, we interpret the processes behind these changes. In particular, we discuss the representation of ground ice and permafrost thawing in the models, and finally we analyze the evolution of boreal wetlands extent based on a reduced subsample of 10 models.

2. Experimental Design

2.1. CMIP6 Climate Models and Data Description

We performed our analysis on an ensemble of CMIP6 simulations run with 14 GCMs which contributed to the historical (Eyring et al., 2016; Meinshausen et al., 2017) and the ScenarioMIP experiments (O'Neill et al., 2016). The historical simulations cover the recent past (1850–2014), they are forced with observed greenhouse gas concentration and estimated land-use changes. The period 1995–2014, included in the historical experiment, is described below as the "present-day period" and constitutes our baseline in the analysis of the wetlands evolutions projected over the period 2015–2100 for different scenarios from ScenarioMIP. The different ScenarioMIP experiments are forced with greenhouse gas concentration scenarios that rely on alternative future narratives (O'Neill et al., 2017) and their implications (Riahi et al., 2017), known as Shared Socioeconomic Pathways (SSPs), which are associated with levels of radiative forcing by 2100. We carry out our study on the four Tier 1 SSPs: SSP1-2.6 ("Sustainability", with a relatively low radiative forcing of 2.6 $W \cdot m^{-2}$), SSP2-4.5 ("Middle-of the road", medium forcing), SSP3-7.0 ("Regional-rivalry", high radiative forcing also driven by high aerosol emissions and land use change) and SSP5-8.5 ("Fossil-fueled development" with very high radiative forcing). In both historical and scenario simulations, the models typically employ an ensemble approach, running multiple realizations known as "members," to quantify and mitigate the uncertainty caused by internal variability. Table 1 presents the 14 GCMs and their land component, along with the number of available ensemble members for each model.

The selection of these models was based on their provision of essential variables required for our study from the CMIP6 archive (see Data Availability Statement). The variables our approach requires are the liquid water content of each soil layer (*mrsll*), the frozen water content of each soil layer (*mrsfl*), and the temperature of each soil layer (*tsl*). We also consider precipitation (*pr*) and evapotranspiration (*evspsbl*) to analyze our results. All these variables are available at a monthly averaging timestep. Furthermore, our approach uses the saturated soil water content (porosity, denoted as w_{sat}) values from the models. While not directly available in the CMIP6 archive, we obtained this variable either directly from the modeling groups or by recalculating it using the equations provided in the model descriptions and referencing SoilGrids data sets for soil properties (Poggio et al., 2021). All variables are remapped for comparisons from their native grid to a common $1° \times 1°$ grid using the first-order conservative method.

2.2. TOPMODEL Calibration

We have adapted the original TOPMODEL concepts (Beven & Kirkby, 1979) to simulate the area covered by wetlands in each grid cell, based on the subgrid topography distribution. The relationship between the wetland fraction and the liquid water content of the grid cell is established as follows (detailed in Appendix A):

Table 1
Model References and Number of Members for Each Experiment

CMIP6 model	Land surface model	Number of members	
		Historical	SSPs
ACCESS-ESM1-5 (Ziehn et al., 2020)	CABLE (Kowalczyk et al., 2006, 2016)	40	10–30
BCC-CSM2-MR (Wu et al., 2019)	BCC-AVIM (Li et al., 2019)	3	1
CanESM5 (Swart et al., 2019)	CLASS-CTEM (Arora et al., 2018)	50	50
CESM2-WACCM (Danabasoglu et al., 2020)	CLM5 (Lawrence et al., 2019)	3	1–3
CMCC-CM2-SR5 (Cherchi et al., 2019)	CLM4.5 (K. Oleson et al., 2013)	1	1
CMCC-ESM2 (Lovato et al., 2022)	CLM4.5 (K. Oleson et al., 2013)	1	1
CNRM-CM6-1 (Voldoire et al., 2019)	ISBA-CTRIP (Decharme et al., 2019)	30	6–9
CNRM-ESM2-1 (Séférian et al., 2019)	ISBA-CTRIP (Decharme et al., 2019; Delire et al., 2020)	10	5–9
GFDL-ESM4 (Dunne et al., 2020)	LM4 (M. Zhao et al., 2018)	1	1
IPSL-CM6A-LR (Boucher et al., 2020)	ORCHIDEE (Krinner et al., 2005)	14	6–11
NorESM2-LM (Seland et al., 2020)	CLM5 (Lawrence et al., 2019)	3	1–3
NorESM2-MM (Seland et al., 2020)	CLM5 (Lawrence et al., 2019)	3	1–2
TaiESM1 (Wang et al., 2021)	CLM4 (W. Oleson et al., 2010)	1	1
UKESM1-0-LL (Sellar et al., 2019)	JULES (Harper et al., 2016, 2018)	16	5–16

Note. A range is given for SSPs if all SSPs do not have the same number of members. The choice of models was conditioned by the provision of essential variables (see text).

$$w_l = w_{\max} - (w_{\max} - w_{\min}) \frac{F(\lambda_{wtl})}{4} \quad (1)$$

where $F(\lambda_{wtl})$ is a function linking the distribution of the topographic index within the grid cell $\Gamma(\lambda)$ to the wetland fraction f_{wtl}. Here, w_l represents the mean annual liquid water content, $w_{\max}$ represents the mean annual maximum soil water content, and $w_{\min}$ represents the mean annual minimum soil water content of the grid cell. These values are computed over the "active layer" depth d_{wtl} (see Appendix A). The active layer corresponds to the depth of the shallowest unfrozen soil layer and is set to a maximum depth of 3 m when there is no frozen layer shallower than 3 m. If the surface top layer is frozen part of the year, the liquid water content and maximum water content are calculated only for the period during which the surface is unfrozen. This approach allows us to consider the specific dynamics of boreal wetlands, which have a shallow active layer that melts seasonally and lies on an impermeable frozen layer.

The minimum water content $w_{\min}$ represents the threshold below which the wetland fraction of the grid cell is set to zero. This threshold can be derived from physical quantities such as the wilting point in the root zone, or the field capacity for a strict wet soil limit. However, these quantities may not always be available, and different models may calculate and define them differently. To address these challenges and account for both soil spatial heterogeneity and model differences, we opted to define $w_{\min}$ as a fraction χ of the maximum water content. In other words, if the liquid water content occupies a volume in the soil greater than $\chi \cdot w_{\max}$, we consider the average deficit of the cell to be small enough to allow the occurrence of wetlands. As a result, Equation 1 can be simplified to:

$$\frac{w_l}{w_{\max}} = 1 - (1 - \chi)\frac{F(\lambda_{wtl})}{4} \quad (2)$$

where χ is a parameter set between 0 and 1. We tested various values for χ within a range of 0.5–0.8, encompassing the values that can be found for the field capacity to porosity ratio, which varies spatially depending on soil properties.

Our preliminary findings demonstrate the ability of the TOPMODEL-based approach to diagnose wetlands (see the Results Section 3.1). However, they also highlight the lack of precision at regional to local scales when considering the multi-model mean. Another drawback of using a uniform parameterization for χ is the substantial variation in wetlands extent observed among the different climate models (Figure S1 in Supporting Information S1). This discrepancy arises because some models already have soil water content close to saturation, making it easier to simulate wetlands with this approach. In contrast, other models exhibit relatively low soil moisture content compared to their maximum capacity, resulting in wetland estimates occurring only in few of the known wetland regions.

To address these limitations, we propose a customized parameterization that considers model-specific characteristics and soil heterogeneity, calibrated using observational data sets.

We selected the WAD2M database (Zhang et al., 2021a) as a calibration baseline because it is the most up-to-date global wetland map, which integrates satellite data sets and statistical approaches with static maps from cross-sources combinations. This data set corresponds to the definition of wetlands we are able to simulate with our approach, that is, areas with saturated soil conditions. WAD2M excludes permanent water bodies such as lakes, rivers and reservoirs, which are generally not considered soil in LSMs and thus are not captured by our approach. Furthermore, WAD2M removes artificial wetlands such as rice paddies, which can also be challenging to simulate with the LSMs because of artificial inundations. WAD2M provides data at a monthly timestep from 2000 to 2020, allowing for a dynamic representation of wetlands extent, which can be divided into categories such as minimum permanent, seasonally inundated, and intermittent wetlands. For our study's requirements, we computed the yearly mean of the WAD2M product for each year, excluding months with frozen ground during which the wetland fraction remains undefined. This approach ensures comparability of the WAD2M with our estimates of mean extent of wetlands, which rely on the mean annual liquid water content during unfrozen soil conditions.

In addition, we removed intermittent and seasonal wetlands that may occur in arid areas by masking these regions in the WAD2M data set. These areas only become wetlands during occasional extreme events of precipitation or inflow (Lehner & Döll, 2004), which may not be fully captured by the models or significantly increase the yearly mean soil water content. We followed the United Nations Environment Program definition and used the Global Aridity Index version 3 data from Zomer et al. (2022) to set the wetland fraction to zero for regions with an aridity index less than 0.2. The arid zones are represented in white in Figure 1 and the following ones.

The common period shared by the CMIP6 historical simulations and the WAD2M database is 2000–2014. To calibrate each model, we computed a single value of χ per grid cell based on the average 2000–2014 conditions, stating:

$$\chi = 1 - \left(1 - \frac{\overline{w_l}}{\overline{w_{\max}}}\right) \frac{4}{F\left(\lambda_{wtl}, \overline{f_W}\right)} \tag{3}$$

where $\overline{w_l}$ and $\overline{w_{\max}}$ respectively represent the yearly averaged liquid water content and porosity simulated by the model over the period 2000–2014. $\overline{f_W}$ is the wetland fraction obtained from WAD2M, also averaged over the same period (2000–2014), and used as input in the function $F(\lambda_{wtl})$. To ensure an accurate representation, particularly in regions with high wetland fractions like the Hudson Bay or the Siberian Lowlands, a small correction was introduced by directly adjusting the upper bound $w_{\max}$ of the model for some of the grid cells. But we chose not to over-calibrate this value to avoid the occurrence of over-saturated soils in these boreal regions in the future climate projections (see in Supporting Information S1 for further details). To obtain more satisfactory results in these areas, we also used a 4-year running average of w_l (see Appendix A) instead of the yearly values of Equation A8.

3. Projections of Wetlands Extent

3.1. Impact of Calibration on Present-Day Accuracy

Figure 1a shows the multi-model mean map averaged over the period 2000–2014 for $\chi = 0.65$, which yields good overall results compared to the map in Figure 1c taken from the WAD2M wetland observation database (Zhang et al., 2021a), also averaged over the same period. The original (not calibrated) version of our approach succeeds

10.1029/2024EF004553

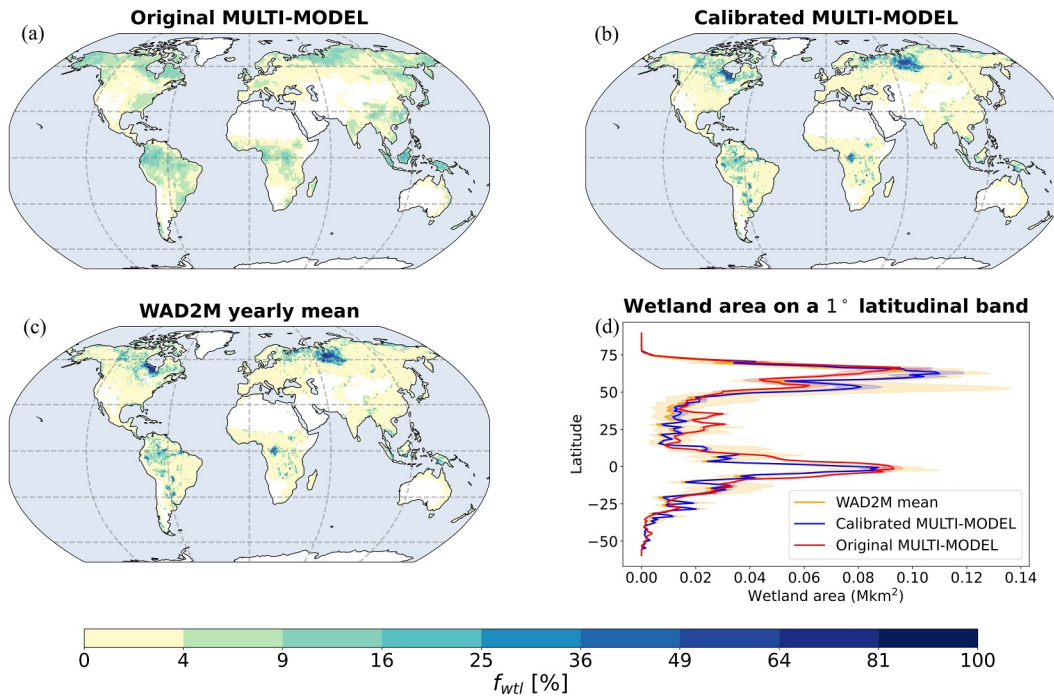

Figure 1. Wetland fraction per grid cell (%) for the original Multi-Model mean with $\chi = 0.65$ (a), the calibrated Multi-Model mean (b), and the WAD2M yearly mean used for calibration (c) averaged over 2000–2014. (d): Wetland area zonal means (Mkm^3) averaged over 2000–2014. The orange shading is delimited by WAD2M's mean annual minimum and maximum computed over the same period.

in simulating the main regions where the extent of wetlands is significant, such as west Siberian lowland, the Hudson Bay, the Amazon basin, the Congo basin, and the Indonesian archipelago. It gives good results when we compare it to the WAD2M zonal means (Figure 1d). However, it fails to accurately simulate the total extent of these areas, generally underestimating the local density of wetlands and overestimating their spatial coverage over larger regions. This anomaly is particularly noticeable in tropical rainforests, where the wetland occurrence is more evenly distributed than observations suggest. In the Arctic, the model fails to simulate the high density of wetlands in the west Siberian and HBL, while wetlands extent in permafrost areas such Alaska and eastern Siberia tends to be higher than observed.

Additionally, the model overestimates wetlands extent in Central-Europe, the Southern United States, and a vast region encompassing India, China, and Southeast Asia. These regions coincide with areas where historical declines in natural wetlands have been particularly significant, as indicated by the findings of Fluet-Chouinard et al. (2023). These populated regions include large rivers basins, where wetlands have been transformed for other land uses, predominantly for agricultural purposes like wetland drainage to establish croplands, or conversion into rice paddies, and other forms of wetland cultivation. This suggests that the overestimation in these areas could be attributed to the inability of our approach to capture the loss of natural wetlands resulting from direct anthropogenic activities.

The improvements obtained with the calibrated parameterization are presented in Figure 1b for the multi-model mean of the wetland fraction over the period 2000–2014 (results by model are shown in the Figure S2 of Supporting Information S1). With this calibration of χ, our approach is able to fully capture the current spatial coverage of wetlands derived from WAD2M for the MULTI-MODEL mean. Some overestimation remains compared to WAD2M when we consider models individually in the regions mentioned above, such as tropical rainforests, Arctic permafrost regions, or areas where historical wetlands losses have occurred. These biases are nevertheless reduced when multi-model averaging is performed.

This slight overestimation is compensated, on zonal average, by a general underestimation of the wetland coverage in the Hudson bay and the WSL which exhibit a very high wetland density (from 50% to 90% of the cell).

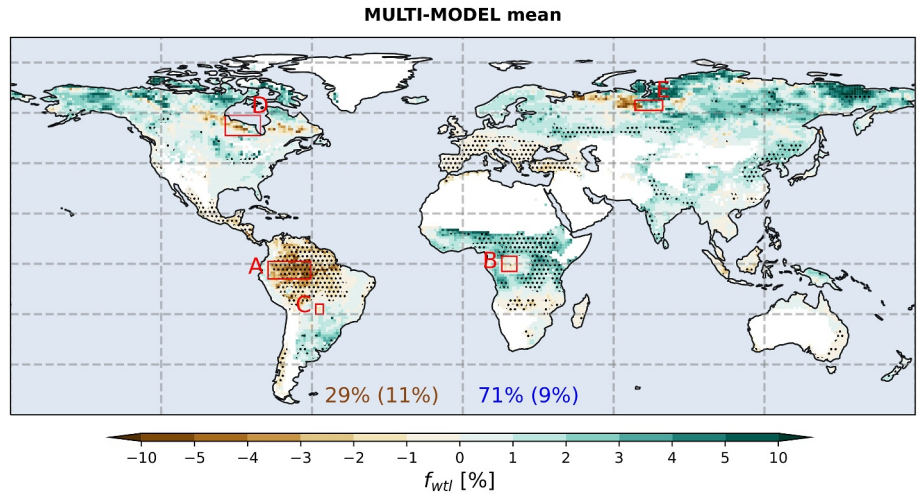

Figure 2. Multi-model mean changes in fraction of wetland area per grid cell (%) between 1995–2014 and 2081–2100 using the SSP370 scenario (future minus present-day period). The dots indicate the locations where at least 80% of the models agree on the sign of the change. The global percentages represent the share of grid cells impacted by negative changes (brown) or positive changes (blue), with values enclosed in brackets when agreement exceeds 80%. The red rectangles correspond to the major global wetlands of the Amazon Basin (a), the Congo Basin (b), the Pantanal (c), Hudson Bay (d) and the Western Siberian Lowlands (e).

In these areas, the multi-model mean estimates are on average 18% lower than the WAD2M fraction, with discrepancies of up to 25% for some grid cells. It appears that our TOPMODEL-based approach is not able to accurately simulate the very high wetland fractions of these grid cells, as this would require liquid soil water contents to remain close to their mean values over the years. However, the multi-model mean remains higher than the WAD2M annual minimum extent in these areas for the period 2000–2014.

This customized parameterization yields much better results than our original TOPMODEL-based approach and provides an accurate representation of current wetlands extent. We have therefore used the calibrated version to compute the extent of wetlands in the 2015–2100 ScenarioMIP experiments.

3.2. Global Shifts in Wetlands Extent

Figure 2 shows the multi-model mean change in wetland area between 1995–2014 and 2081–2100 for SSP370. Overall, 71% of the areas considered show an increase, and 29% a decrease. These values are lowered to 9% and 11% respectively when we consider only areas with more than 80% agreement, which indicate opposite estimates from the models, especially in regions where the multi-model mean shows an increase. A gain in wetlands is simulated over most parts of the high and mid-latitudes of the northern hemisphere, with generally less than 80% of models that agree on the sign of change, except in some regions in Central North America, Eastern Europe, South Western Siberia and Eastern Siberia. An increase in wetlands extent, with sparsely good agreement between models, is also observed in East Asia, South Asia and eastern South America. More than 80% of models agree on an increase in wetlands extent in Central, Eastern and Western Africa, to the exception of the Congo Basin, where a slight drop is simulated by less than 80% of the models. Other losses with a low model agreement occur in Eastern and Central Canada, northwestern Russia, and parts of South–East Asia. Losses with a strong model agreement are simulated in the Mediterranean and western Europe, the northern part of southern Africa, central America and the region that encompasses the major wetlands of the Amazon basin. The overall trend shows an increase in wetlands extent between the present-day period and the end of the 21st century, whatever the SSP scenario (Table 2).

We also analyzed the behavior of five of the largest wetlands (Keddy et al., 2009), framed in red on Figure 2. This list is composed of two equatorial wetlands: the Amazon Basin (a) and Congo Basin (b), one tropical wetland: the Pantanal (c), and two boreal wetlands: the HBL (d) and the WSL (e). While the global extent of wetlands is on the rise, we noted that these major wetlands are all showing signs of decline across at least over a portion of their area.

Table 2
Global and Regional Wetland Area (in 10^3 km^2) Over the Present-Day Period (1995–2014) and Projected Over the 2081–2100 According to the Four SSPs

	Present	SSP126	SSP245	SSP370	SSP585
Global extent	3,747	3,799	4,016	4,347	4,443
Beyond 50°N	1,698	1,782	1,939	2,081	2,155
Western Amazon Basin	188	156	147	136	129
Congo Basin	97	94	94	96	99
Pantanal	32	31	31	31	31
Hudson Bay	148	139	139	145	146
Western Siberian Lowlands	121	117	123	122	121

3.3. Changes in Major Wetland Complexes

Figure 3 shows the evolution of the largest global wetlands mentioned above between 1950 and 2100, based on the multi-model mean. However, since this represents an average across a model ensemble, the depicted inter-annual variability is notably lower than that simulated by each individual model and is solely a depiction of the long-term trend. The left panel of Figure 3 specifies the distribution, average, median, variability and significance of all models projected changes between the present-day period (1995–2014) and the long term period (2081–2100). The current areas of wetlands and their evolution according to the different SSPs over the long-term are presented in Table 2. Table S2 in Supporting Information S1 shows the location in coordinates and the total area of the regions considered.

Figure 3a presents the evolution of the western and central part of the Amazon River Basin, from the Andes up to the confluence with the Rio Negro. This equatorial basin is mainly made up of the tropical rainforest eco-region, characterized by warm temperatures and high annual rainfall rates (Marengo, 2004). The mostly flat terrain, combined with high precipitation levels, leads to the presence of extensive wetlands (Gumbricht et al., 2017; Junk et al., 2011). In the studied parts of the basin, more than 85% of the catchment area is forested (Melack & Hess, 2011). As a result, the wetlands correspond mainly to whitewater and blackwater floodplain forests, and to a lesser extent to flooded savannahs and swamps (Junk et al., 2011). Some of these wetlands are classified as peatlands, that is, areas where peat, a layer containing a high proportion of organic matter, is present (Gumbricht et al., 2017; Melton et al., 2022). A decrease of wetlands extent is shown for all SSP scenarios, ranging from—17% (SSP126) to −31% (SSP585) for the mean value of the 2081–2100 period, compared to 1995–2014. However, the large interquartile range (IQR) (27% on average) indicates a wide dispersion of models for all the scenarios. For the SSP245, SSP370 and SSP585 scenario, 13 models out of 14 present a significant decrease, suggesting a robust projection on the sign of change. Only SSP126 shows conflicting changes, with the majority of models (11) still indicating a decrease in wetlands.

Results for the Congo Basin are shown in Figure 3b. This basin is the second largest equatorial basin after the Amazon, and is also mostly covered by tropical rainforest. It also has high rainfall, although lower than that of the Amazon, with two seasonal peaks corresponding to the north–south migration of the tropical rainbelt (Alsdorf et al., 2016). A depression in the central part known as the "Cuvette Centrale" contains extensive wetlands, mostly swamp forests with dense canopy (Bwangoy et al., 2010; Gumbricht et al., 2017). An important difference, compared to the Amazon basin and its floodplains, is that the wetlands of the Central Cuvette sit at a higher elevation than the level of the adjacent Congo River, so these wetlands are less dependent on annual variations in river level (Lee et al., 2011, 2015). Consequently, almost half of the Cuvette Centrale is covered by peatlands, mostly ombotrophic, making it the largest area of lowland tropical peatlands (Crezee et al., 2022; Dargie et al., 2017). Wetlands extent shows a slight but conflicting decrease according to SSP126 and SSP245 (−3%), unsignificant decrease according to SSP370 and a slight conflicting increase for SSP585 (+2%). Despite the overall small average change, there is high dispersion among models, which intensifies with the severity of the scenario, ranging from an IQR of 11% for SSP126 to 23% for SSP585. Interestingly, as radiative forcing increases, more models predict an increase in wetlands extent, with the number of models showing this trend rising from four under SSP126 to seven under SSP585, and eight (though less significantly) under SSP370. This inversion in sign of change in some models may be attributed both to a change or increase in rainfall regime over the basin and the impact of land use changes, particularly deforestation, which can reduce evapotranspiration and enhance soil water content in certain model simulations.

Figure 3c shows the evolution for the Pantanal, considered as the largest continuous tropical wetland. The main basin is a depression in the upper part of the Paraguay River, situated 15–20° south of the equator. The wetland relies on an important flood pulse, driven by the rainfall regime in the Amazon region, where headwaters are initiated and flow toward the lowland floodplain (Junk & Cunha, 2005). In addition to the seasonal cycle between the wet and dry seasons, the Pantanal is subject to considerable inter-annual and multi-annual variability (Ikeda-Castrillon et al., 2020; Nunes da Cunha & Junk, 2004). Savannas (Cerrado) predominates in 50% of the Pantanal, but the region also contains steppic (semi-arid) savannas (Chaco), semi-deciduous and deciduous seasonal forests, and pioneer formations in permanently or semi-permanently flooded habitat (grasslands, floating meadows,

10.1029/2024EF004553

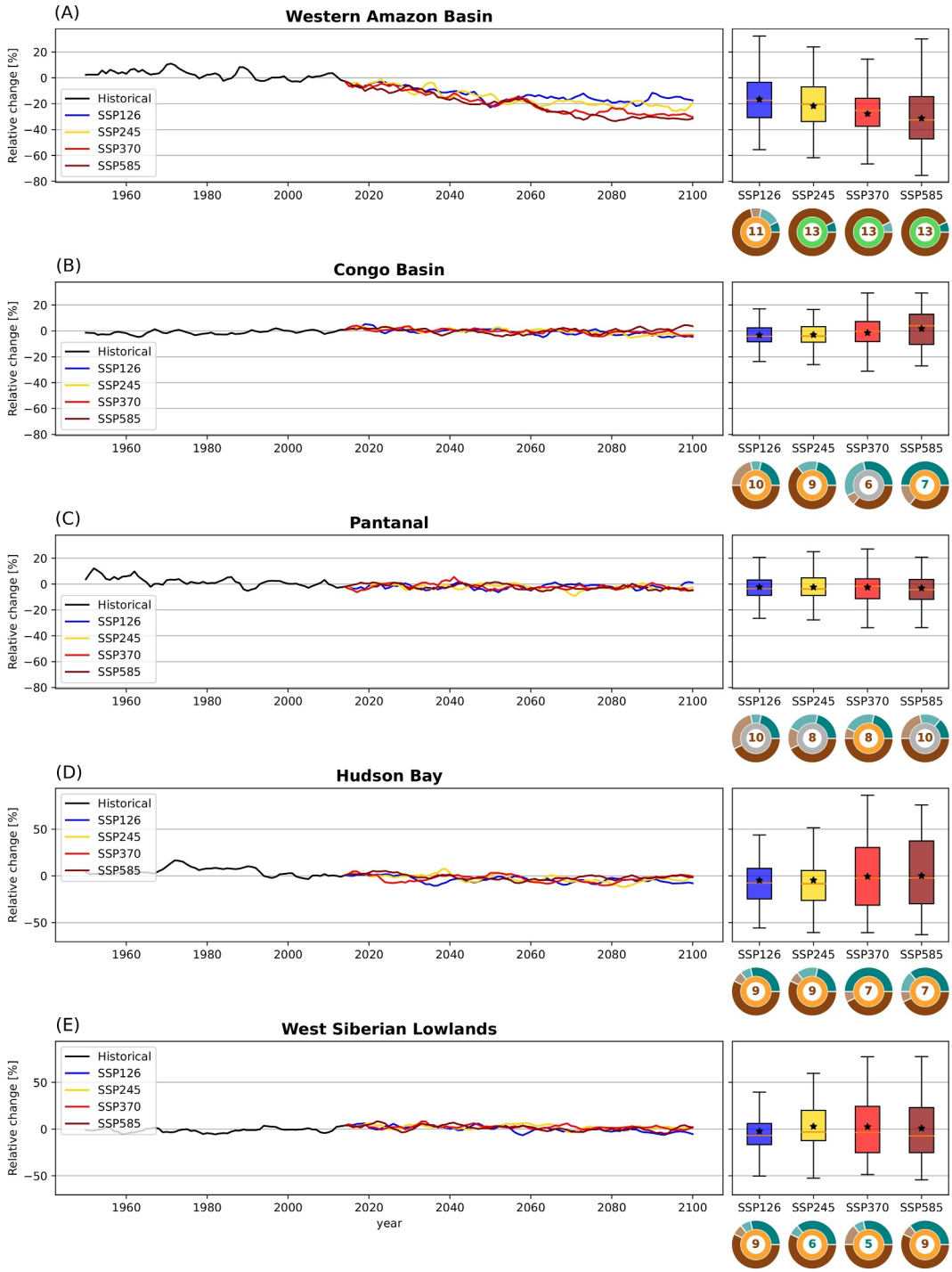

Figure 3. Left column: Time series (1950–2100) of multi-model mean wetlands extent anomalies (relative to the present-day period (1995–2014)) for Amazon Basin (a), Congo Basin (b), Pantanal (c), Hudson Bay (d), and West Siberian Lowlands (e) under four shared socioeconomic pathways (SSPs). Right column: Box plots of changes [(2081–2100)—(1995–2014)] for each model in the same regions and for each SSPs. The boxes indicate the first and third quartiles, the whiskers show values comprised within 1.5 times the interquartile range (IQR), the orange bar is the multi-model median and the black star the multi-model mean. Below each box plot, is shown the number of models sharing the sign of the multi-model trend mean. The outer circle of the donut chart shows the share of models projecting a positive (blue) or negative change (brown), with bright (shaded) colors indicating the share of models with a statistically significant (not significant) change (see in Supporting Information S1 for definition of the statistical significance). The inner circle's color indicates significance of the multi-model change. Green: 66% of models show a significant change with 80% of models agreeing on the sign of change. Orange: 66% significance with less than 80% inter-model agreement. Gray: Less than 66% significance.

swamps) (Pott et al., 2011). Our results show a slight and non-significant decrease of the wetlands extent for SSP126, SSP245 and SSP585. SSP370 present a conflicting decrease, with seven models showing a decrease and three an increase that exceeds their variability threshold. The number of model presenting a significant increase is lowered for SSP585, leading to a greater but unsignificant decrease. We believe that the high natural internal variability of rainfall in the Pantanal may explain why few models show a significant change in the extent of wetlands. The dispersion is quite high and increases slightly with the scenario (12%–15%).

The evolution of the HBL is presented Figure 3d. The HBL is the third largest wetland complex in the world (Keddy et al., 2009). It is located in the south of the Hudson Bay and west of the James Bay, mainly in Manitoba and Ontario (Canada). Despite its relatively low latitude (between 51°N and 59°N), the climate in HBL is abnormally cold, mainly due to the cooling effect of the sea ice. There is nevertheless a strong north–south temperature gradient, colder on the north coast with a subarctic marine climate, and warmer inland and south in the boreal climate zone (Rouse, 1991). There is a band of continuous permafrost along the north coast, while there are discontinuous and sporadic transitional bands inland, and even a permafrost-free zone in the south (Olthof & Fraser, 2024). More than 80% of the HBL is covered by wetlands, with a tundra landscape in the north, dominated by thin layers of peat and fen along the coast and polygonal peatbogs further inland, a boreal forest with wooded peat bogs in the south and a transition zone of peatland and swamp in between (Dredge & Dyke, 2020). This large complex dominated by peatlands is one of the greatest pool of soil organic carbon on Earth (Hugelius et al., 2014; Loisel et al., 2014; Sothe et al., 2022). The multi-model mean of projections shows a slight decrease of wetlands extent for SSP126, SSP245, which is even smaller for SSP370 and SSP585. However, models display conflicting results in every scenario, with a clear sign opposition between models (see donut-plot). Between seven and nine models agree with the sign of the change, which means that another non-negligible group of models (half or almost) project a sign of change that is opposite to the multi-model mean. This inter-model dispersion increases sharply as radiative forcing increases, with an IQR of around 32% for the SSP126 and SSP245, 62% for SSP370, and 67% SSP585. This high IQR value indicates that, as well as being opposite, the changes projected by the models may be very strong in the Hudson Bay wetlands.

Finally, Figure 3e shows the evolution of part of the WSL, the largest wetland complex in the world. Here, we only consider the region located between 61 and 65°N, which has the highest occurrence of wetlands. This region is marked by a cold, continental climate, with the presence of a discontinuous and sporadic permafrost (Kremenetski et al., 2003). In the Taiga region, peat bogs with a variety of landforms are the dominating type of wetlands (Zakharova et al., 2014), with numerous lakes of varying sizes (Karlsson et al., 2021; Polishchuk et al., 2018). A forested tundra vegetation with the presence of big frozen peat mounds is found in the north of our region (Kremenetski et al., 2003). The peatlands of the Siberian plains form a very large pool of organic carbon (Hugelius et al., 2014; Sheng et al., 2004). As in the case of HBL, the multi-model mean shows nearly no change in the extent of wetlands (see Table 2), but the models show conflicting results, with significant changes for models predicting an increase and those predicting a decrease. In particular, the multi-model trend shows a slight increase for SSP245 and SSP370, but respectively only six and five models agree on a positive sign of change. This means that a minority of models, but predicting a mean stronger increase, influence the sign of the multi-model mean. There is also nearly no change of the multi-model mean in the SSP585 scenario, while nine models show a decrease (significant for eight of them) and five models show a significant increase. The dispersion is also high and increases with the severity of the scenarios: 22% for the SSP126, 32% for SSP245, and almost 50% for SSP370 and SSP585. Thus, the apparently small changes shown by the multi-model mean for the HBL and WSL hide strong and opposite changes between the models.

4. Climate Drivers of Changes in Wetlands Extent

4.1. Changes in Precipitation and Evapotranspiration

In order to explain the projected evolution of wetlands extent, it is necessary to examine the processes driving these changes. With our TOPMODEL-based approach, the wetlands extent is diagnosed using the liquid soil water content. It corresponds to a share of the total soil water content, which is equal to the total water content when the soil remains thawed throughout the year. Water input through precipitation and losses to the atmosphere through evapotranspiration are the main fluxes that control the soil water content. Although the mean annual precipitation over land is predicted to increase in all scenarios, there is a strong spatial variability, with only slight changes in certain regions and a significant decrease in others (Douville et al., 2021). Evapotranspiration changes

are driven by precipitation changes and changes of the evaporative demand from the atmosphere, which increases with the rise in temperature (Dai et al., 2018). The role of vegetation is complex; while the increase in atmospheric CO_2 tends to improve plant water use efficiency (Milly & Dunne, 2016), the additional vegetation and lengthening of the growing season in mid to high latitudes increase the water demand (Mankin et al., 2019). Projected land use and land cover changes also directly affect evapotranspiration. However, changes in evapotranspiration fluxes are most often strongly correlated with changes in precipitation in regions experiencing significant precipitation changes (See Costantini et al. (2023) for an example with CMIP6 models).

Figure 4 shows the changes of mean annual precipitation (P), evapotranspiration (E) and P–E between 1995–2014 and 2081–2100 for SSP370. It is consistent with previous studies using CMIP6 models (Cook et al., 2020; Costantini et al., 2023; Douville et al., 2021). Small differences may exist with these studies, which are due to our sub-sample of 14 climate models, compared to the entire panel or other sub-samples. In particular, we have a better agreement in precipitation decrease over the Amazon basin and in some mid-latitudes regions than the IPCC AR6 findings (Masson-Delmotte et al., 2021). In our case, the high model agreement in mean annual P and P–E decrease over the Amazon basin explains very well the decrease in soil water content and therefore wetlands extent previously shown. There is also a good agreement between the CMIP6 models on a decrease in soil moisture, in line with our results (Parsons, 2020).

Only small changes with low model agreement occur for the multi-model mean of annual P and E in the central Congo basin. Divergence in sign and amplitude on annual precipitation changes between models participating in CMIP5 was also reported for central Africa (Aloysius et al., 2016). Almazroui et al. (2020) with CMIP6 models show small changes in annual precipitation for central Africa for SSP126 and SSP245, and a slight increase for SSP585, which correlates well with our estimate of wetlands extent. The poor agreement between models on the evolution of wetlands extent in the Congo Basin can be explained by the high uncertainty of the evolution of the multi-model mean of P, E and P–E. Furthermore, we note that the annual sign of P–E is slightly positive, while a slight negative change is observed for the evolution of wetlands for the SSP370 scenario. A drying up of the soil with low robustness is also reported in the literature (Cook et al., 2020). We believe that this is due to the influence of climate change on vegetation growth, and to the land use changes which are quite significant in this region and whose influence is therefore likely to be strong (Hurtt et al., 2020). However, these two changes are only taken into account by Earth System Models (as opposed to GCMs which do not all include interactive vegetation schemes and land use changes) and have different impacts on wetlands from one model to another.

The Pantanal shows an even smaller change in the sign of P–E, while P and E both present a slight decrease, and we find a low model agreement on all of these changes. As in the Congo Basin, this lack of agreement between the models and the small changes in P and P–E explain the small changes in the extent of wetlands shown by the multi-model mean. The slight decrease in precipitation can explain the slight decrease in evapotranspiration and induces the mean decrease of soil water content. This decrease in rainfall is likely to have a smaller impact than that of direct human pressures on the Pantanal wetlands (Marengo et al., 2016), such as land-use change caused by deforestation and the rapid development of agro-industrial activities, or the construction of numerous dams for hydroelectric power generation and irrigation (Ikeda-Castrillon et al., 2020).

In the high and mid-latitudes of the northern hemisphere, both P and E are expected to increase, with a good agreement between models, as depicted on Figure 4. Variations in the value of P–E changes are smaller and depend on the difference in the rates of increase of P and E. However, there are greater uncertainties regarding the sign of P–E changes in the region extending from the mid-latitudes to the approximate permafrost transition zone. This includes the large boreal wetlands of the Hudson Bay (HBL) and the WSL. While the low model agreement on P–E may explain the conflicting results on wetlands extent in these regions (Figure 3), the low values of P–E changes do not explain the significant increase and decrease of wetlands extent shown individually by the models in these areas.

4.2. Contrasting Trends in Liquid Water Content at High Latitudes

Previous studies (Berg et al., 2017; Cook et al., 2020) have shown that the water content decreases in the upper soil layers in wide regions of the high latitudes, which include extensive wetlands areas (HBL and WSL regions). Projections of water content over the whole soil column tend to show an increase, albeit with higher uncertainty. This divergence stems from marked seasonality in P–E changes despite the low annual changes. In summer, evapotranspiration increases due to warmer temperatures, primarily affecting the upper soil layers owing to

10.1029/2024EF004553

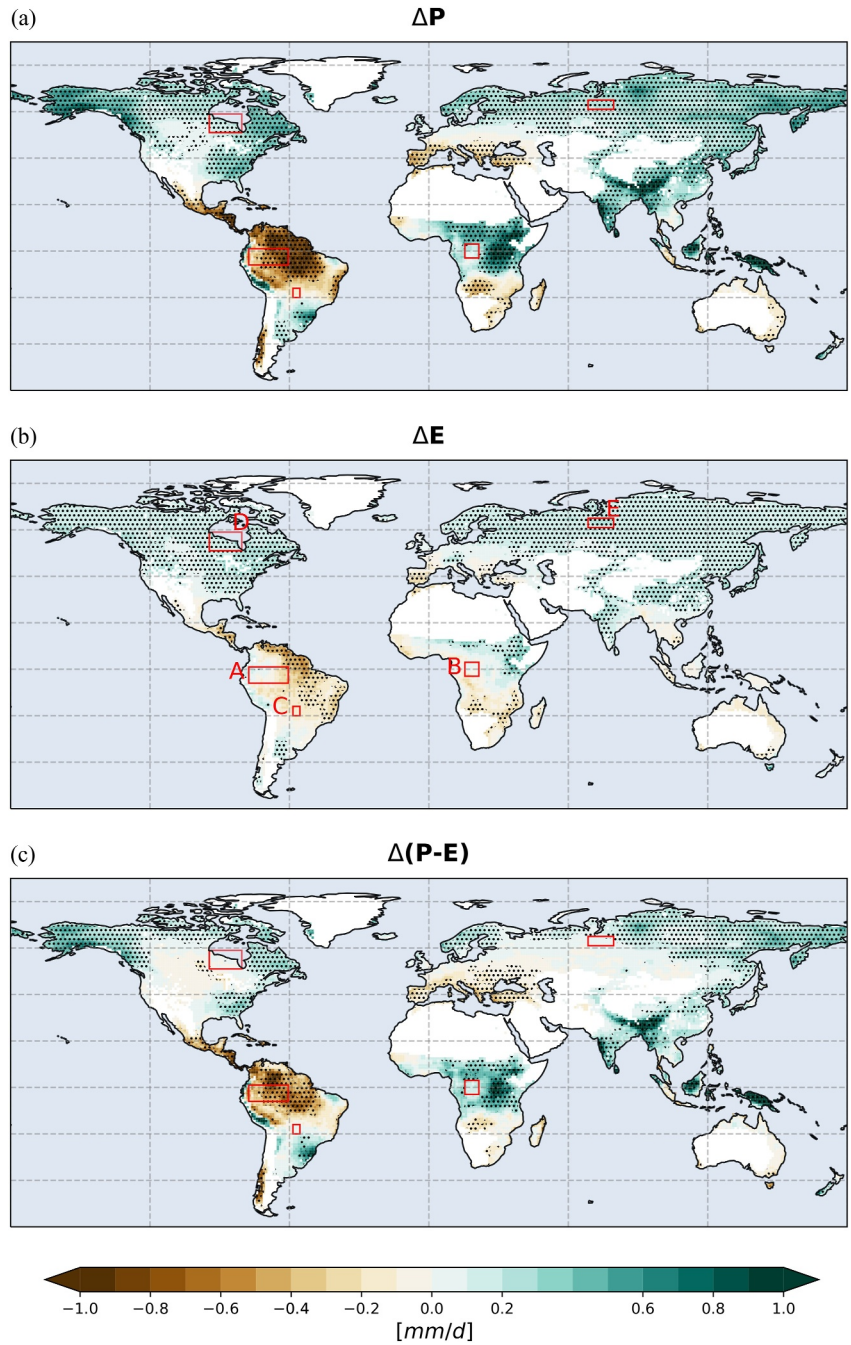

Figure 4. Multi-Model mean changes in precipitation (a), evapotranspiration (b) and precipitation minus evapotranspiration (c) between 1995–2014 and 2081–2100 according to the SSP370 scenario. The dots indicate locations where at least 80% of the models agree on the sign of change.

shallow root depths of vegetation and relatively slow upward capillary flow. In contrast, the increased precipitation in winter tends to have a stronger impact on deeper layers. Cook et al. (2020) shows that the CMIP6 multi-model mean demonstrates better agreement compared to CMIP5 for surface drying in the Hudson Bay and WSL regions in both seasons. Conversely, the water content over the total column increases, but with less agreement than for the surface in the CMIP6 multi-model mean.

Figure 5 shows the changes in liquid soil water content beyond 50°N between the present-day period and 2081–2100 for the SSP370 scenario. It reveals a large discrepancy between the models and in between regions, which

10.1029/2024EF004553

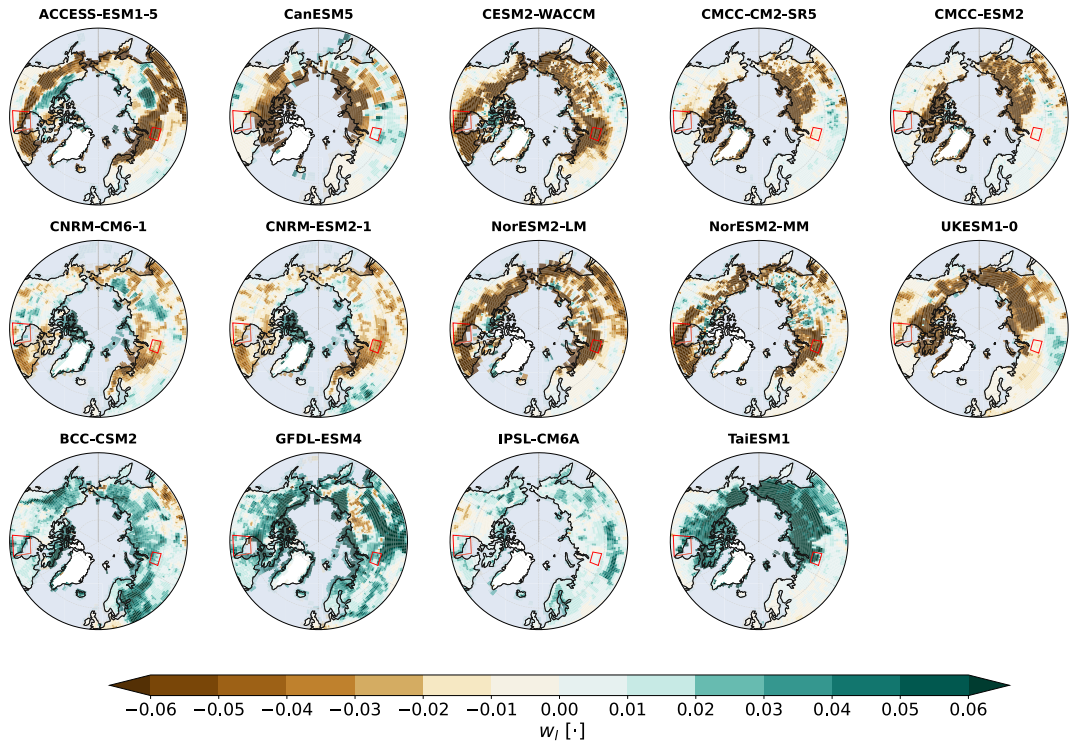

Figure 5. Mean changes in soil liquid water content between 1995–2014 and 2081–2100 for each model according to the SSP370 scenario beyond 50°N. The 10 models where the liquid water content increases on average are shown in the first two rows, and the four where it decreases in the last row.

explains the low model agreement in wetlands extent we found in the northern high latitudes (Figure 3). There are also major differences in the magnitude of these changes, regardless of their sign.

We note that four models, BCC-CSM2, GFDL-ESM4, IPSL-CM6A and TaiESM1 (in the bottom of Figure 5), show an increase in liquid water content in the vast majority of boreal regions. The results of the other 10 models (ACCESS-ESM1-5, CanESM5, CESM2-WACCM, CMCC-CM2-SR5, CMCC-ESM2, CNRM-CM6-1, CNRM-ESM2-1, NorESM2-LM, NorESM2-MM and UKESM1-0) are more spatially heterogeneous, but they all agree on a significant decline in Siberia and in the northern regions of North America. For at least half of this second group of models, it appears that the areas where the liquid water content falls sharply correspond to the permafrost transition zones, where it is currently considered to be sporadic or discontinuous. Liquid water content changes in the current continuous permafrost, especially in eastern Siberia, are more ambiguous but they can present a significant decrease. It should be noted that the representation of thermal processes in models is highly variable, leading to a simulated extent of permafrost that does not necessarily correspond to current observations (Burke et al., 2020; Koven et al., 2013).

The models behave similarly across all SSPs beyond 50°N with the same four models simulating an increase in w_l while the 10 others a decrease (Figure S5 in Supporting Information S1). Generally, higher radiative forcing in the SSP scenarios correlates with greater increases in w_l for the four models showing an upward trend, and greater decreases in w_l for the 10 models exhibiting a downward trend.

Quite similar behaviors are observed for the evolution of the global liquid water content (Figure S6 in Supporting Information S1). The amplitude of the globally averaged variations are of the same order of magnitude as those averaged beyond 50°N, meaning that the changes of w_l in northern regions strongly influence the overall global change. These variations are the primary source of discrepancy between models regarding annual liquid water content changes, and consequently for changes in global wetlands extent in our diagnosis. At the global scale, a larger radiative forcing does not necessarily indicate a larger change in w_l, suggesting that changes of varying signs and magnitudes between regions can counteract each other. Additionally, one model from the group of 10 that exhibits a decrease in liquid water content beyond 50°N, CNRM-CM6-1, shows little variation in the globally

10.1029/2024EF004553

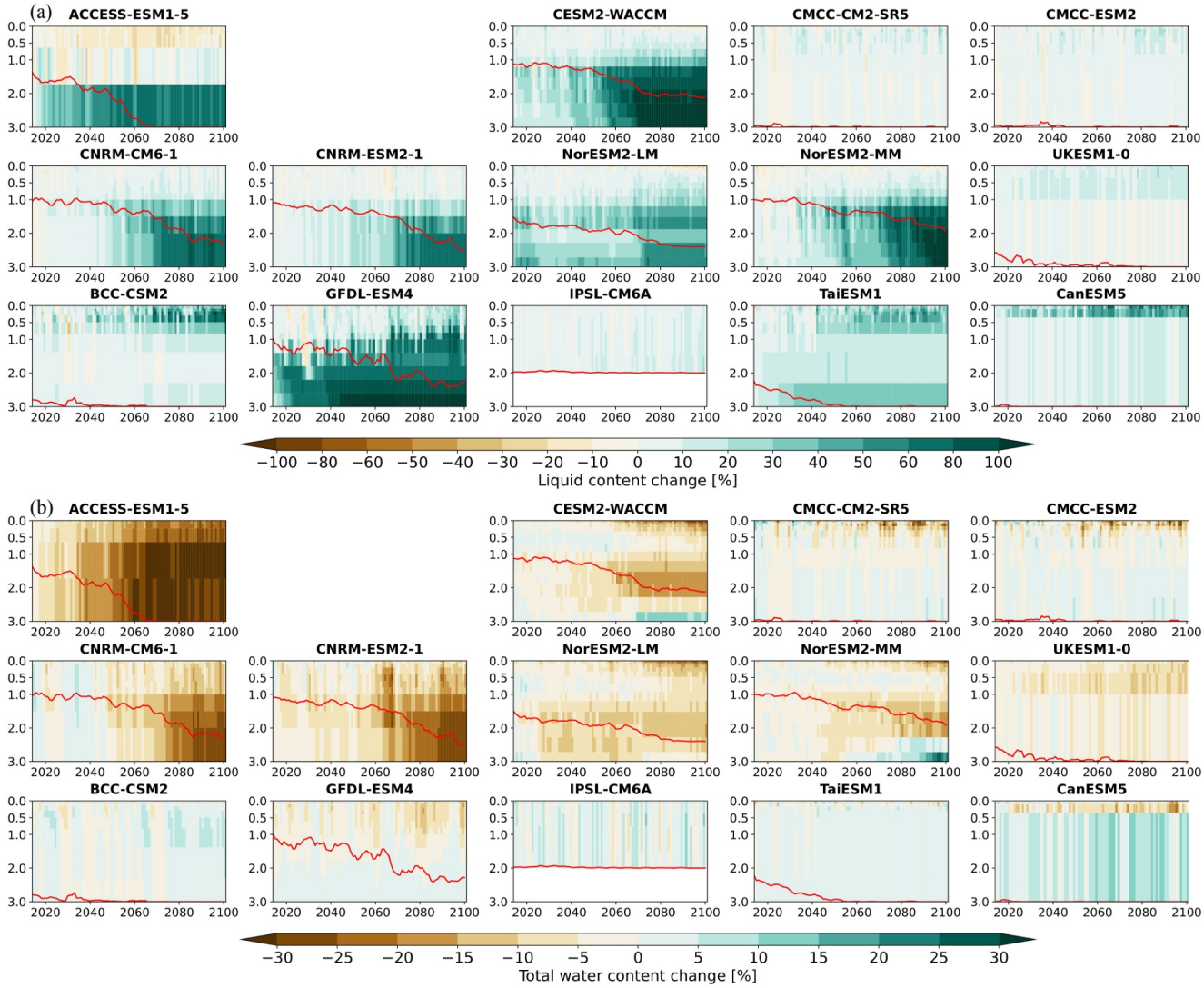

Figure 6. Vertical profile of changes along the years (from 2015 to 2100, compared to 1995–2014) in the mean annual liquid water content (a) and total water content (b) in the Western Siberian Lowlands for each model according to the SSP370 scenario. The red line corresponds to the mean annual depth of unfrozen soil d_{wtl} when the surface is not frozen.

averaged w_l. Nevertheless, because it shares the same physical parameterizations as CNRM-ESM2-1, which consistently shows a decrease across all SSP scenarios, we classify it within the group of models indicating drying conditions.

In the following subsection, the models are separated in two groups as we further analyze and discuss their contrasted behavior. The four models showing an increase of soil liquid water content are referred to as "group W" (wetting), and the 10 models showing an averaged drying are referred to as "group D" (drying).

4.3. Impacts of Permafrost Thawing Across Model Groups

To explain the contrasted projections of boreal wetlands extent between models in group *W* (BCC-CSM2, GFDL-ESM4, IPSL-CM6A and TaiESM1) and *D* (ACCESS-ESM1-5, CanESM5, CESM2-WACCM, CMCC-CM2-SR5, CMCC-ESM2, CNRM-CM6-1,CNRM-ESM2-1, NorESM2-LM, NorESM2-MM and UKESM1-0), we investigate their differences in projected changes in liquid, ice and total water content. Figure 6 presents for each model the evolution of the liquid water content vertical profile (a) and total water content vertical profile (b), spatially averaged on the WSL region in the SSP370 scenario. The changes are computed using the annually

averaged CMIP6 variables *mrsll* and *mrsol* from 2015 to 2100, compared to the 1995–2014 average. The annual mean depth of the unfrozen layer (d_{wtl}), shown in red, only considers values where the surface has thawed. The nine models showing a decrease in wetland extent for WSL are displayed in the top two rows. The last row shows the four W models showing a generalized increase in w_l at high latitudes, along with CanESM5 that also project and increase in the WSL.

All models exhibit distinct behaviors that require an examination of the physical processes represented by each. Nevertheless, it can be observed that among the models showing an increase in w_l, three or even four models (BCC-CSM2, IPSL-CM6A, CanESM5 and to a lesser extent TaiESM1) exhibit a relatively stable active layer depth, remaining close to its maximum value of 3 m (2 m for IPSL-CM6A). This suggests these models simulate little to no permafrost in the WSL, where the ground freezes during winter but thaws rapidly and completely during the growing season when temperatures rise above freezing. For TaiESM1 (and to a lesser extent BCC-CSM2),permafrost is simulated in the coldest parts of WSL, which forms a transition zone. This explains why the average "active layer" d_{wtl} is relatively deep in the present-day period and deepens further in response to climate change.

These four models also exhibit a notable increase in liquid water content (Figure 6a), particularly in upper soil layers. This can be due to an increase in atmospheric input (precipitation minus evapotranspiration), but also because of ice melting (see Figure S8 in Supporting Information S1 for the evolution of ice fraction). Ice melting is caused by warming and the lengthening of the growing season, which leads to an increase in annual liquid water content relative to the ice content in the layer. Additionally, it can make the soil more permeable, enhancing the infiltration of precipitation and snowmelt on the surface and increasing percolation into lower layers. In BCC-CSM2 and TaiESM1, w_l also increases in deeper layers as d_{wtl} increases over time due to ice melting from frozen layers into liquid water (Figure S8 in Supporting Information S1).

There is a slight surface decrease in total water content (Figure 6b) for TaiESM1 and CanESM5, suggesting an increased rate of evapotranspiration or percolation. However, total water content remains constant or slightly increases in deeper layers for these four models. This indicates that surface water input is not fully compensated by increased drainage to deeper layers. Given the stable active layer depth, minimal changes in total water content, and increased liquid water fraction, it logically follows that w_l increases in these four models.

GFDL-ESM4, part of the group W models showing an increase of w_l, represents permafrost in the WSL region, requiring separate discussion. GFDL-ESM4 shows a strong increase in liquid water at the surface, and an even stronger increase below the d_{wtl} layer (Figure 6a), probably caused by ice melting. The total water content decreases at the surface but remains largely unchanged around d_{wtl} (Figure 6b), suggesting increased surface evaporation and percolation but little or no increase in drainage. Unfortunately, we cannot directly confirm this hypothesis as there is no output of drainage for GFDL-ESM4. While the total water content changes little, the increase in w_l is less straightforward than for other group W models, as the active layer depth also increases. This suggests an annual influx of additional liquid water into the active layer, not just a relative increase from ice melting. Thus, thawing of permafrost raises the water table depth, as drainage does not fully compensate for the surface inflow increase.

The majority of group *D* models (ACCESS-ESM1-5, CESM2-WACCM, CNRM-CM6-1, CNRM-ESM2-1, NorESM2-LM, NorESM2-MM) show an increase in the fraction of liquid water (Figure 6a). This increase is primarily relative to the ice content and is caused by the deepening of d_{wtl} and ice melting. The surface liquid water content increases slightly or decreases, even if the annual liquid/ice ratio rises due to warming (Figure S8 in Supporting Information S1), suggesting that surface inflow of liquid water is low or negative after evapotranspiration is subtracted from precipitation. This is confirmed by the marked decrease in total water content at the surface and around d_{wtl} (Figure 6b). Thawing of the impermeable layer increase drainage, resulting in a loss of total water content to underlying layers or rivers. This is illustrated in the CESM2-WACCM and NorESM2 models, which show an increase in total water content in the layers below d_{wtl}. In contrast, ACCESS-ESM1-5 and the CNRM models exhibit greater and deeper total water loss and an accelerated increase in the unfrozen layer thickness, likely due to faster ground warming and a deeper annual maximum in summer. Thus, according to these models, the thawing of permafrost results in the drying of WSL, as surface inflows are insufficient to counterbalance increased drainage and sub-surface runoff.

The drying simulated by the CMCC models and UKESM1-0 does not seem to be explained by increased drainage in the bottom layers caused by permafrost thawing. These models present an increase in liquid water content near the surface with low changes below (Figure 6a), while total water content decreases in the surface layer and even below for UKESM1-0 (Figure 6b). It is assumed that in these models, the increase in mean annual liquid water near the surface is due to greater ice and snow melting, but the total water balance is negative due to a greater increase of the evapotranspiration than precipitation rate. The rapid increase in evapotranspiration may also affect the deeper layers in UKESM1-0, which has only four layers. For these models, changes in precipitation and evapotranspiration fluxes, combined with a slight deepening of the active layer compared to the present-day period, explain the drying of the WSL. Note that the CMCC models show only a very slight decrease in w_l in the WSL, consistent with the minimal changes in liquid and total water content by layer.

A similar analysis can be applied to the HBL (Figure S9 in Supporting Information S1), leading to comparable conclusions. The WSL and HBL are characterized by sporadic to discontinuous permafrost, occasionally continuous in the coldest zones. This characteristic may explain why some models represent little or no permafrost in these regions, and why we find important average values of d_{wtl} that increase rapidly in response to global warming. We also investigate areas with continuous permafrost, such as the Eastern Siberian Lowlands (ESL) (Figure S10 in Supporting Information S1). Here, the depth of the unfrozen layer (d_{wtl}) is approximately 1 m for all the models of group *D* at the beginning of the 21st century. The rapid increase of d_{wtl} observed in CMCC models and UKESM1-0 results in enhanced drainage to lower layers, contributing to the decrease in w_l in these three models. In contrast, other Group *D* models show a slower increase in d_{wtl}, indicating greater resilience of permafrost to thawing. This small change in the depth of the unfrozen layer, combined with an increase in atmospheric input, leads for example, to an increase in w_l for ACCESS-ESM1-5 and the CNRM models in the ESL.

To sum up, our analysis of the boreal regions of ESL, HBL and WSL emphasize the dominant role of frozen layer dynamics in shaping the evolution of liquid water content within the active layer at high latitudes. Extensive thawing of the frozen layer can enhance permeability and increase drainage toward lower layers. This leads to a reduction of available liquid water (lowering of the water table) when surface water increase is outweighed by concurrent drainage increase. Conversely, if the frozen layer is resilient to thawing, and drainage increases little compared to atmospheric input, models show that liquid water content increases (rising water table). However, while our analysis provides insights into the effects of permafrost thaw on the water content of the active layer, it reveals significant sources of uncertainties not only regarding atmospheric changes, but also the speed of thawing and deepening of the active layer. This highlights the critical need to enhance the representation of permafrost and soil processes in Land Surface Models.

5. Refined Projections of Boreal Wetlands Extent Using Permafrost-Compatible Models

Although the group *D* models have different representations of the permafrost processes and simulate different permafrost extent, they all show that changes in w_l depend on complex interactions between changes in precipitation, evapotranspiration, and soil thawing. Therefore, we narrow our focus to the response of the 10 group *D* models in northern high-latitude regions. This decision is supported by their representation of hydrological processes linked to permafrost and ice melting that seem better adapted to boreal regions. Moreover, these models are in agreement with CMIP6 average findings in the HBL and WSL, where drying trends in the upper 10 cm have been found (Cook et al., 2020).

Figure 7a shows the evolution of the wetlands extent in HBL when we consider only the 10 models of group *D*. Unlike what was shown on Figure 3d with all 14 models, we now find a net decrease of the multi-model mean wetlands extent throughout the 21st century in all SSPs. The long-term change (2081–2100 minus 1995–2014) is of the same order of magnitude in every scenario, between −19% for SSP126 and—23% for SSP585. While the average loss increases only very slightly with an increase of the radiative forcing, the inter-model dispersion notably widens for SSP370 and SSP585 (IQR of 52%) compared to SSP126 (25%) and SSP245 (33%). This dispersion indicates significant variability among models in response to increasing radiative forcing, with some showing decreases and others increases in wetlands extent. Most projections suggest a decrease in wetlands extent with greater warming, although some models suggest a potential increase relative to present-day conditions under scenarios with higher radiative forcing. It can be seen in the agreement between the models, since nine out of 10

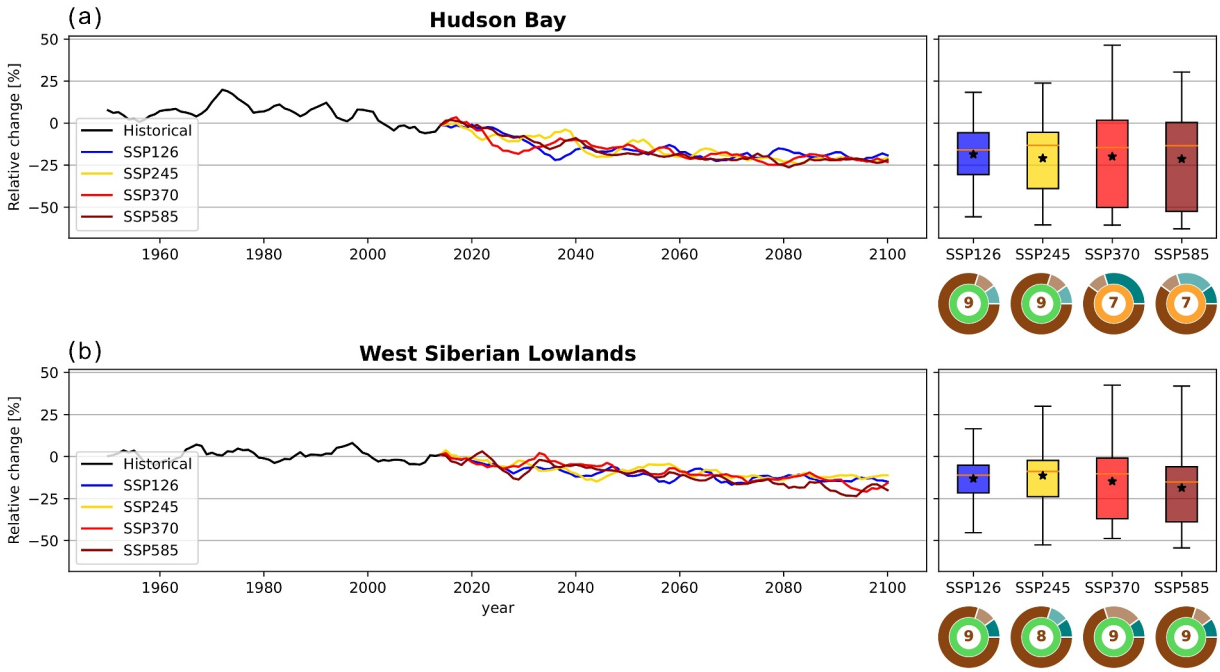

Figure 7. Same figure as 3 for the Hudson Bay Lowlands (a) and the West Siberian Lowlands (b) using only the 10 models of group D.

models show a decrease in wetlands extent (eight significant) for SSP126 and SSP245, whereas only seven out of ten (six significant) are observed for SSP370 and SSP585, leading to conflicting changes. Interestingly, there are three models that show a significant increase for the SSP370, while only one for the SSP585. Nevertheless, a decrease in wetlands extent, at least in the medium term (2041–2060) or under mitigated global warming, appears very likely in the HBL according to group *D* models.

The evolution of wetlands extent in WSL, presented in Figure 7b, also indicates a net decrease with a good agreement between the models. The changes ranges from −12% for SSP126 and SSP245 to −19% for SSP585. Only one model of Group *D* presents a significant increase in the region for all the SSPs (CanESM5, as discussed with Figure 6). For the remaining models, there is robust model consensus across all SSPs, with seven models projecting a significant decrease in wetlands extent for SSP370 and eight models for SSP126, SSP245, and SSP585. The IQR increases from 16% for SSP126 to 36% for SSP370. A significant decrease in wetlands extent is therefore projected in the WSL according to group *D* models.

The evolution of wetland extent, as indicated by the group *D* multi-model mean, is detailed in Table 3, which presents present-day and long-term projections for each SSP averaged globally, beyond 50° North, and across the HBL and WSL regions. Changes in the Amazon Basin, Congo Basin, and the Pantanal are not included, as they do not substantially differ from the values in Table 2 that include group W models. Furthermore, excluding group W models in tropical regions where permafrost and frozen water content are not relevant is not justified. Comparing with Tables 2 and 3 shows a decrease in wetland extent relative to the present-day period, both globally and in northern high latitudes. However, the magnitude of this change is not proportional to the radiative forcing of SSPs. We find a greater loss of wetlands with less severe scenarios on a global scale. This suggests that the rate of wetland disappearance accelerates more rapidly than the rate of their creation as temperatures rise. This phenomenon may occur because some wetlands, experiencing a decrease in extent due to warming, reach critical minimum values. This could happen either because they completely disappear or because they transform in response to new hydrological conditions, such as transitioning into permafrost-free wetlands in boreal regions.

Table 3
Global and Regional Averages of Wetland Area (in 10^3 km^2) for the Present-Day Period (1995–2014) and the Long-Term Period (2081–2100) According to the Four SSPs for the Group D Multi-Model Mean

	Present	SSP126	SSP245	SSP370	SSP585
Global extent	3,746	3,437	3,500	3,635	3,609
Beyond 50°N	1,724	1,479	1,502	1,494	1,449
Hudson Bay	150	121	117	118	116
Western Siberian Lowlands	123	107	109	105	100

The geographic distribution of changes in wetland extent projected by the group *D* models is depicted in Figure 8, illustrating the multi-model mean

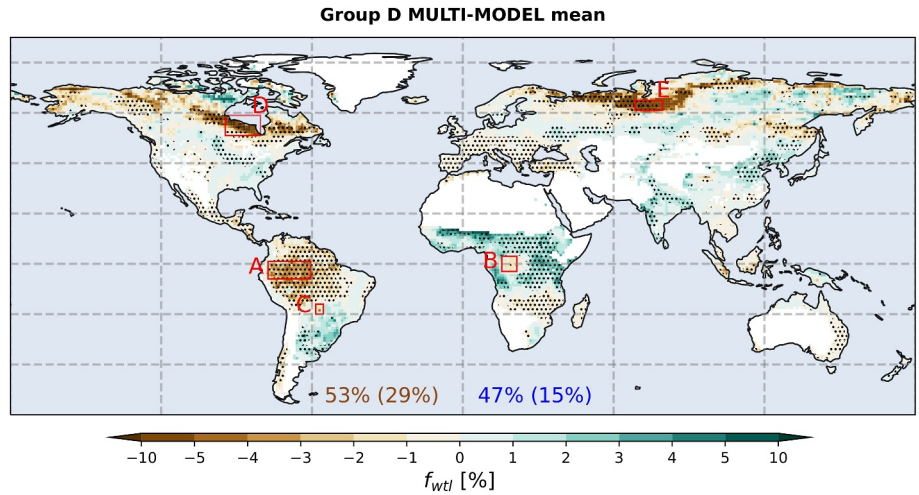

Figure 8. Map of group D multi-model mean changes in fraction of wetland area per grid cell between 1995–2014 and 2081–2100 using the SSP370 scenario. The dots indicate the locations where at least 80% of the models agree on the sign of the change. The global percentages represent the share of grid cells impacted by negative changes (brown) or positive changes (blue), with values enclosed in brackets when agreement exceeds 80%. The red rectangles correspond to the major global wetlands of the Amazon Basin (a), the Congo Basin (b), the Pantanal (c), Hudson Bay (d) and the Western Siberian Lowlands (e).

long-term change in the SSP370 scenario. In contrast to Figure 2, which included all 14 models, the updated figure now shows more grid cells experiencing a decrease (53%) than an increase (47%). There is also improved model agreement, covering over 44% of the land surface compared to 20% previously, with 29% of the surface where models concur on a decrease and 15% where they agree on an increase. As expected, there are minimal differences observed for equatorial to subtropical regions in terms of sign and magnitude of change, as well as agreement between models.

The main differences occur at temperate and boreal latitudes. A gain in wetlands extent, with good model agreement, is observed in Central North America, Eastern Europe, and South Western Siberia, whereas a significant decrease is observed in a large part of the boreal zone, particularly encompassing the major wetlands of the HBL and WSL. The region that includes the HBL extends northwest into the Canadian Shield taiga, and east into central Nord-du-Québec and Labrador. Similarly, the sharp decline in wetlands extent observed in the WSL also encompasses a large part of northwestern Russia and northern Fennoscandia to the west, and extends to the northeast along the Yenissei and Khatanga river basins. In both cases, there is good model agreement across most of these areas. A smaller decline, with good model agreement, is also observed in northwestern Canada and southern Eastern Siberia. Decreases are also reported in Alaska and the northeast of Eastern Siberia, albeit with lower model agreement. In permafrost regions, wetlands extent is projected to increase only in Nunavut and the central part of Eastern Siberia with low model agreement, and in parts of the ESL with good model agreement.

By narrowing our model ensemble based on physical criteria, we observe a significantly different trend beyond 50°N, showing a general decrease in boreal wetlands extent and much better model agreement. These results suggest that a generalized increase in boreal wetlands extent is unlikely, while a decrease in the extent of the major boreal wetlands is more probable, despite the projected increase in precipitation in high northern latitudes. We argue that permafrost thawing, combined with changes in atmospheric input, will control the evolution of boreal wetlands. If permafrost thaw leads to an increase in total runoff, particularly deep drainage, it should result in drying of the active layer and a reduction in wetlands extent if the increase in atmospheric input is insufficient. However, significant uncertainties remain, especially in continuous permafrost regions where resilience to thawing may be greater.

The likely reduction in the extent in boreal wetlands, particularly WSL and HBL regions, could potentially have local repercussions on climate, hydrological, and ecological processes. In particular, these wetlands encompass many northern peatlands (Hugelius et al., 2014), which are large carbon reservoirs (Loisel et al., 2014, 2017). If these peatlands experience partial drying due to global warming, it could significantly impact the carbon cycle, as

oxic decomposition of accumulated peat could potentially transform northern peatlands into sources of CO_2 before 2100 (Huang et al., 2021; Hugelius et al., 2020; Voigt et al., 2019; B. Zhao & Zhuang, 2023).

6. Discussion

6.1. Additional Effects of Permafrost Thawing

Observational studies show that the low-flow of Arctic rivers is increasing (Rennermalm et al., 2010; Smith et al., 2007; Walvoord & Striegl, 2007), and that the area of lakes is decreasing, particularly in the discontinuous permafrost zone (Smith et al., 2005; Webb & Liljedahl, 2023). This supports the notion that the thawing of the permafrost and the active layer deepening leads to an increase in subsurface drainage. Additionally, the thawing permafrost not only amplifies drainage, but also alters the topography and landscape of boreal regions (Czudek & Demek, 1970; Osterkamp et al., 2000; Quinton et al., 2011; Rowland et al., 2010). Thawing of the frozen soil influences its structural integrity, causing subsidence and the collapse of surface layers, a phenomenon known as thermokarst (Farquharson et al., 2019; Grosse et al., 2013). The emergence of unfrozen zones (taliks) is reshaping the hydrographic network, introducing new lateral and horizontal flows, along with shifts in water storage dynamics (Connon et al., 2014; Walvoord & Striegl, 2007).

While these dynamics support the idea that thawing permafrost tends to dry out existing wetlands, they also highlight certain limitations in our study. First, our approach based on a current topographic index distribution does not take into account the changes in topography caused by the thawing of the permafrost. Second, these changes may lead to the local transition of existing wetlands, such as peatlands lying on an impermeable frozen layer, to young thermokarst lakes (Kokelj & Jorgenson, 2013; Mamet et al., 2017). These transitioning wetlands have a significant impact on the carbon cycle, as in the short term, young thermokarst lakes have low vegetation and are methane sources, while dried out peatlands can generate peat decay and release significant amount of CO_2 (Hugelius et al., 2020). The decay of the peat layer may also result in a reduced thermal insulation of the underlying soil, which can accelerate permafrost degradation. This feedback loop is not taken into account in most Earth System Models, as they do not include a dynamic representation of peatlands.

6.2. Effects of Seasonal Cycle and Inter-Annual Changes

Variations in the seasonal and inter-annual cycles, particularly the increased frequency of extreme droughts and floods, could significantly impact the extent of wetlands. However, our goal was to emphasize long-term robust changes. We therefore chose to filter out sudden variations with a 4-year temporal filter (see Appendix A) and to use multi-model means. This method does not allow to capture seasonal and inter-annual variability and misses potential extreme drought events, which is a limitation given their impact.

Lázaro et al. (2020) shows that precipitation and flooded area are decreasing since the 1970s in the Pantanal, particularly during the dry season. Extreme drought events have been recently observed in the Pantanal (Marengo et al., 2021), and the magnitude and frequency of these events could increase according to climate change projections, but still with a high uncertainty (Marengo et al., 2016). This increase in seasonal variability and drought extremes has also been reported in the Amazon for the present-day period and are projected for the future (Marengo & Espinoza, 2016; Parsons, 2020). The changes observed in the Congo Basin appear to be less pronounced and spatially heterogeneous, but climate models also project variations in the seasonal cycle and episodes of extreme floods and droughts (Creese et al., 2019; Karam et al., 2022).

These variations in the seasonal cycle, and the increase in periods of drought and flooding, can affect ecosystem diversity, wetlands biophysical processes, and consequently the carbon cycle (Nunes da Cunha & Junk, 2004; Olivares et al., 2015). As for the boreal peatlands, the carbon stored in tropical peatlands may be released into the atmosphere in the form of CO_2 instead of being accumulated with a lowering of the water table (Garcin et al., 2022).

6.3. TOPMODEL-Based Approach in Flat Terrain

Using the topographical hydrological model TOPMODEL to predict wetlands in flat areas has limitations due to its assumption that the hydraulic gradient is proportional to the slope. This assumption is less accurate in flat areas where the slope is minimal (Beven et al., 2021; Beven & Kirkby, 1979), which can result in potential inaccuracies in wetlands extent prediction. This issue, noted for example, in the Pantanal by Gloor et al. (2021), could also

apply to the Hudson Bay and WSL. In these three areas, we have observed that strong calibration is necessary to accurately represent wetlands extent for the present-day period. While calibration can partially mitigate these issues, a model that accounts for soil heterogeneity, carbon and vegetation dynamics, ice presence, and other processes controlling subsurface flow would undoubtedly be more suitable for these regions. Although this simplified TOPMODEL-based approach may introduce errors in the amplitude of changes, these errors are likely insignificant within the context of a multi-model analysis due to wide model dispersion. Additionally, these errors do not affect the sign of change, which is primarily determined by variations in soil liquid water content.

7. Conclusion

In this study, we developed an approach based on a topographic hydrological model to diagnose wetlands extent in simulations run with Global Climate Models and Earth System Models. We analyzed the variation of wetlands extent in response to climate change from 1950 to 2100, using a multi-model ensemble of CMIP6 simulations (historical and SSPs scenarios). We used a calibration parameter adapted to each model to insure a realistic distribution of wetlands in the present-day period. To improve our diagnosis of boreal wetlands extent, we calculated the depth of the active layer to take into account thawing of permafrost in response to global warming.

We showed that the 14 CMIP6 models we considered agree on a strong loss of wetlands in the Amazon basin in response to future climate change. In the western part of the basin, we reported losses ranging from −22% for the SSP245 scenario to −28% for SSP370 by the end of the 21st century. For the Congo and Pantanal wetlands, depending on the scenarios, we found either conflicting results, with models not agreeing on the sign of change, or unsignificant changes. In the rest of equatorial Africa, models agree on an increase in the extent of wetlands, while in Central America, southern Africa and Western Europe, models agree on a reduction of wetlands extent.

We then selected a sub-sample of 10 models that better represent the consequences of permafrost thaw on the water content of the active layer. With this group of models, we found a long-term loss in wetlands extent of −20% for the HBL, and −15% for the Central Siberian Lowlands under the SSP370 scenario. We also showed that these wetland losses extend widely to the northern high latitudes in the permafrost transition zones, with a generally good model agreement. According to this sub-sample of models, the extent of wetlands could be reduced by 13% beyond 50° N by the end of the 21st century. These contrasting results highlight the significant uncertainties that remain related to the representation of permafrost in Land Surface Models and its evolution with climate change.

Even if the future of wetlands on a global scale remains uncertain, our study underlines that climate change has the potential to significantly reduce the extent of large wetland complexes, while concurrently giving rise to emerging wetlands in some areas. This transformation could have strong implications on local energy and water exchanges, ecosystems, and on the carbon cycle, which would thereby affect climate change itself with both positive and negative feedbacks. Conversely, certain processes, such as thermokarst-induced alterations in topography, peat thermal insulation, or water retention capacity, could alter the response of wetlands extent to climate change, and are yet not accounted for in our diagnostic approach. To improve our understanding of climate change's influence on wetlands extent, and to assess its potential feedbacks on the Earth system, we argue that Global Climate Models and Earth System Models should incorporate a more explicit representation of wetlands. Nevertheless, it should be noted that although climate change significantly impacts wetlands extent, direct human activities which are not represented in climate models, such as wetland artificialization or drainage, remains a significant and highly uncertain factor, which have dramatically affected wetlands extent in the past.

Appendix A: TOPMODEL-Based Approach Description

Although TOPMODEL was initially designed for large watersheds (Beven & Kirkby, 1979), it has been extended for use in larger areas such as global or regional land surface models (Decharme et al., 2006; Gedney & Cox, 2003; Habets & Saulnier, 2001). The model represents runoff generation by dynamic contributing area, assuming that sub-surface flow is the primary factor generating saturated areas.

To determine the saturated-soil fraction of the watershed, a relationship is established between the depth of the mean saturation front (the mean water table depth) and the distribution of spatial heterogeneities in topography and soil properties within the catchment (Sivapalan et al., 1987). The ability of a pixel, represented as unit "i" in the watershed, to become "flooded" is determined by its topographic index λ_i:

$$\lambda_i = \ln\left(\frac{\alpha_i}{\tan\beta_i}\right) \tag{A1}$$

where α_i represents the drainage area per unit of contour, and tan β_i approximates the local hydraulic gradient, with β_i being the local surface slope. Thus, a larger drainage area and lower slope result in a higher ability of the pixel to become saturated. For our study, we use the topographic index distribution provided by the data set of Marthews et al. (2015b), which was calculated from the Digital Elevation Model (DEM) HydroSHEDS (Lehner et al., 2008) with a resolution of 15 arcsec.

In the original TOPMODEL equation, the evolution of the pixel's local deficit $d_{i,t}$, relative to the mean water deficit of the catchment D_t, can be described in relation to the topographic index:

$$D_t - d_{i,t} = -M\left(\bar{\lambda} - \lambda_i\right) \tag{A2}$$

here $\bar{\lambda}$ represents the average value of the topographic index over the catchment or grid cell, while M is a coefficient that characterizes the exponential decrease of soil transmissivity.

The parameter M is often treated as a globally or locally adjustable factor in most recent studies that employ TOPMODEL concepts for representing wetlands (Stocker et al., 2014; Xi et al., 2021; Zhang et al., 2016). In this study, we introduce a different type of parameterization as detailed below. We utilize a value of $M = d_0/4$, where d_0 is the maximum local deficit, as defined in Habets and Saulnier (2001). This maximum local deficit, denoted as the upper limit of the local deficit in the alternative TOPMODEL correction developed by Saulnier and Datin (2004), ensures that the local deficit remains below or equal to the soil surface ($0 \le d_{i,t} \le d_0$).

Using this formulation, the entire area of the grid cell can be divided into three categories: the dry zone, the wet area, and the saturated area, which we will refer to as the wetlands area. This wetlands area corresponds to pixels where the topographic index is above a certain threshold value, denoted as λ_{wtl}. The wetland fraction is then determined by integrating the spatial distribution of the topographic index between λ_{wtl} and the maximum index of the grid cell ($\lambda_{\max}$):

$$f_{wtl} = \int_{\lambda_{wtl}}^{\lambda_{\max}} \delta(\lambda_i) d\lambda_i \tag{A3}$$

As in Ringeval et al. (2012) which is derived from Decharme et al. (2006), we adopt the well-established approach introduced by Sivapalan et al. (1987), which employs a three-parameter gamma function to represent the spatial distribution of the topographic index $\delta(\lambda_i)$. This function is derived from the mean, standard deviation, and skewness of the actual distribution.

The relationship between the mean water deficit D_t and the topographic index threshold is established through the correction proposed by Saulnier and Datin (2004). The formulation is as follows:

$$\frac{D_t}{M} = F(\lambda_{wtl}) = \left(1 - f_{wtl} - f_0\right)\left[\lambda_{wtl} - \overline{\lambda'}\right] + f_0\frac{d_0}{M} \tag{A4}$$

where f_0 represents the dry fraction, and $\overline{\lambda'}$ denotes the mean topographic index over the wet area. For a detailed derivation of these equations, see Appendix A in Decharme and Douville (2006).

As proposed by Habets and Saulnier (2001) and Decharme and Douville (2006), the maximum local deficit is expressed as the difference between the maximum soil water content $w_{\max}$ and a minimum soil water content $w_{\min}$:

$$d_0 = (w_{\max} - w_{\min}) \cdot d_{wtl} \tag{A5}$$

d_{wtl} represents the hydrologically "active" soil depth considered in our study of wetlands extent. Each model features varying soil depths ranging from 2 to 12 m for hydrology (see Table S1 in Supporting Information S1),

making direct comparison of soil moisture content and properties challenging. To address this, we adopt a maximum depth of 3 m (2 m for IPSL-CM6-A, which doesn't have deeper soils) to compute our variables. We make this choice as many models do not extend their soils beyond 3–4 m. Even if they do, the root zone rarely extends deeper, limiting the exchanges with the surface.

Additionally, in high latitudes, a large proportion of the soils are frozen during winter, with thawing occurring at the top during summer. This leads to an easily saturated layer underlain by an impermeable frozen table, promoting wetland occurrence (Kreplin et al., 2021; Woo & Young, 2006).

To account for this permafrost effect, we calculate d_{wtl} for each month as the minimum value between 3 m and the depth z of the last unfrozen layer ($j_{\max}$). We define $j_{\max}$ as the deepest layer j with positive soil temperature $tsl(j)$, and an ice content $mrsfl(j)$ less than 10% of the total water content $mrsll(j) + mrsfl(j)$:

$$d_{wtl} = \min\left(z(j_{\max}), 3m\right),$$
$$\text{with } j_{\max} = \max j \left| \begin{cases} tsl(j) > 273.15°K \\ \dfrac{mrsfl(j)}{mrsll(j) + mrsfl(j)} < 0.1 \end{cases} \right. \tag{A6}$$

when the surface top-layer of the cell is frozen, $d_{wtl} = 0$, indicating that wetlands are not active for that month. The monthly values are then averaged over the entire year, but only for the months when the active layer is defined, allowing us to consider only the growing season in high latitudes.

Using Equation A5, we can calculate the mean water deficit as an expression of the soil liquid water content of the column, denoted as w_l:

$$0 \le D_t = (w_{\max} - w_l) \cdot d_{wtl} \le d_0 \tag{A7}$$

Here, w_l is computed monthly for each model and averaged over the year for the months when d_{wtl} is not null:

$$w_l = \frac{\sum_{j=1}^{j_{\max}} mrsll(j)}{d_{wtl}} \tag{A8}$$

Likewise, the monthly soil maximum content is computed as the weighted sum of the porosity of each layer over $d_{wtl} \neq 0$:

$$w_{\max} = \frac{\sum_{j=1}^{j_{\max}} w_{sat}(j) \cdot \Delta z(j)}{d_{wtl}} \tag{A9}$$

we compute the non-centered 4-year moving average of the annualized values of w_l and $w_{\max}$ to reduce the effects of inter-annual variability in liquid water content on changes in wetlands extent. This allows us to take into account the resilience of wetlands, and ensure that changes in spatial cover are the result of medium and long-term climate trends.

Finally, by substituting $D_t = M \cdot F(\lambda_{wtl})$ from Equation A4 and $M = d_0/4$ into Equation A7, we establish a relationship between the saturation fraction and the liquid water content of the grid cell:

$$w_l = w_{\max} - \frac{M \cdot F(\lambda_{wtl})}{d_{\max}} = w_{\max} - (w_{\max} - w_{\min}) \frac{F(\lambda_{wtl})}{4} \tag{A10}$$

Data Availability Statement

All data from CMIP6 simulations used in our analyses are freely available on the Earth System Grid Federation website (https://esgf-node.ipsl.upmc.fr/search/cmip6-ipsl/). The Wetland Area and Dynamics for Methane Modeling (WAD2M) data set is freely available at (Zhang et al., 2021b). The SoilGrids soils data used to compute

porosity is freely available at https://files.isric.org/soilgrids/latest/data_aggregated/5000m/. Global Aridity Index is freely available at (Zomer et al., 2019). High-resolution global topographic index values is freely available at (Marthews et al., 2015a). The computation scripts and wetland fraction data sets are freely available at (Hardouin et al., 2024).

Acknowledgments
The authors would like to thanks Ian Harman, David Lawrence, Weiping Li, Sergey Malishev, Eddy Robertson and their colleagues for sharing the soil porosity data or the means of obtaining it for the models considered in this study. This work is supported by the "Centre National de Recherches Météorologiques" (CNRM) of Météo-France and the "Centre National de la Recherche Scientifique" (CNRS) of the French research ministry. Additional support was provided by the European Union's Horizon 2020 (H2020) research and innovation program under Grant Agreement No. 101003536 (ESM2025-Earth System Models for the Future).

References

Almazroui, M., Saeed, F., Saeed, S., Nazrul Islam, M., Ismail, M., Klutse, N. A. B., & Siddiqui, M. H. (2020). Projected change in temperature and precipitation over Africa from CMIP6. *Earth Systems and Environment*, *4*(3), 455–475. https://doi.org/10.1007/s41748-020-00161-x

Aloysius, N. R., Sheffield, J., Saiers, J. E., Li, H., & Wood, E. F. (2016). Evaluation of historical and future simulations of precipitation and temperature in central Africa from CMIP5 climate models. *Journal of Geophysical Research: Atmospheres*, *121*(1), 130–152. https://doi.org/10.1002/2015JD023656

Alsdorf, D., Beighley, E., Laraque, A., Lee, H., Tshimanga, R., O'Loughlin, F., et al. (2016). Opportunities for hydrologic research in the Congo Basin. *Reviews of Geophysics*, *54*(2), 378–409. https://doi.org/10.1002/2016RG000517

Arora, V. K., Melton, J. R., & Plummer, D. (2018). An assessment of natural methane fluxes simulated by the CLASS-CTEM model. *Biogeosciences*, *15*(15), 4683–4709. https://doi.org/10.5194/bg-15-4683-2018

Bardgett, R. D., Freeman, C., & Ostle, N. J. (2008). Microbial contributions to climate change through carbon cycle feedbacks. *The ISME Journal*, *2*(8), 805–814. https://doi.org/10.1038/ismej.2008.58

Berg, A., Sheffield, J., & Milly, P. C. D. (2017). Divergent surface and total soil moisture projections under global warming. *Geophysical Research Letters*, *44*(1), 236–244. https://doi.org/10.1002/2016GL071921

Beven, K. J., & Kirkby, M. J. (1979). A physically based, variable contributing area model of basin hydrology/Un Modèle à base physique de zone d'appel variable de l'hydrologie du Bassin versant. *Hydrological Sciences Bulletin*, *24*(1), 43–69. https://doi.org/10.1080/02626667909491834

Beven, K. J., Kirkby, M. J., Freer, J. E., & Lamb, R. (2021). A history of TOPMODEL. *Hydrology and Earth System Sciences*, *25*(2), 527–549. https://doi.org/10.5194/hess-25-527-2021

Boucher, O., Servonnat, J., Albright, A. L., Aumont, O., Balkanski, Y., Bastrikov, V., et al. (2020). Presentation and evaluation of the IPSL-CM6A-LR climate model. *Journal of Advances in Modeling Earth Systems*, *12*(7), e2019MS002010. https://doi.org/10.1029/2019MS002010

Bousquet, P., Ringeval, B., Pison, I., Dlugokencky, E. J., Brunke, E.-G., Carouge, C., et al. (2011). Source attribution of the changes in atmospheric methane for 2006–2008. *Atmospheric Chemistry and Physics*, *11*(8), 3689–3700. https://doi.org/10.5194/acp-11-3689-2011

Bridgham, S. D., Cadillo-Quiroz, H., Keller, J. K., & Zhuang, Q. (2013). Methane emissions from wetlands: Biogeochemical, microbial, and modeling perspectives from local to global scales. *Global Change Biology*, *19*(5), 1325–1346. https://doi.org/10.1111/gcb.12131

Bullock, A., & Acreman, M. (2003). The role of wetlands in the hydrological cycle. *Hydrology and Earth System Sciences*, *7*(3), 358–389. https://doi.org/10.5194/hess-7-358-2003

Burke, E. J., Zhang, Y., & Krinner, G. (2020). Evaluating permafrost physics in the Coupled Model Intercomparison Project 6 (CMIP6) models and their sensitivity to climate change. *The Cryosphere*, *14*(9), 3155–3174. https://doi.org/10.5194/tc-14-3155-2020

Bwangoy, J.-R. B., Hansen, M. C., Roy, D. P., Grandi, G. D., & Justice, C. O. (2010). Wetland mapping in the Congo Basin using optical and radar remotely sensed data and derived topographical indices. *Remote Sensing of Environment*, *114*(1), 73–86. https://doi.org/10.1016/j.rse.2009.08.004

Cherchi, A., Fogli, P. G., Lovato, T., Peano, D., Iovino, D., Gualdi, S., et al. (2019). Global mean climate and main patterns of variability in the CMCC-CM2 coupled model. *Journal of Advances in Modeling Earth Systems*, *11*(1), 185–209. https://doi.org/10.1029/2018MS001369

Clark, D. B., & Gedney, N. (2008). Representing the effects of subgrid variability of soil moisture on runoff generation in a land surface model. *Journal of Geophysical Research*, *113*(D10), D10111. https://doi.org/10.1029/2007JD008940

Connon, R. F., Quinton, W. L., Craig, J. R., & Hayashi, M. (2014). Changing hydrologic connectivity due to permafrost thaw in the lower Liard River Valley, NWT, Canada. *Hydrological Processes*, *28*(14), 4163–4178. https://doi.org/10.1002/hyp.10206

Cook, B. I., Mankin, J. S., Marvel, K., Williams, A. P., Smerdon, J. E., & Anchukaitis, K. J. (2020). Twenty-first century drought projections in the CMIP6 forcing scenarios. *Earth's Future*, *8*(6), e2019EF001461. https://doi.org/10.1029/2019EF001461

Costantini, M., Colin, J., & Decharme, B. (2023). Projected climate-driven changes of water table depth in the world's major groundwater basins. *Earth's Future*, *11*(3), e2022EF003068. https://doi.org/10.1029/2022EF003068

Creese, A., Washington, R., & Jones, R. (2019). Climate change in the Congo basin: Processes related to wetting in the December–February dry season. *Climate Dynamics*, *53*(5), 3583–3602. https://doi.org/10.1007/s00382-019-04728-x

Crezee, B., Dargie, G. C., Ewango, C. E. N., Mitchard, E. T. A., Emba, B. O., Kanyama, T. J., et al. (2022). Mapping peat thickness and carbon stocks of the central Congo Basin using field data. *Nature Geoscience*, *15*(8), 639–644. https://doi.org/10.1038/s41561-022-00966-7

Czudek, T., & Demek, J. (1970). Thermokarst in Siberia and its influence on the development of lowland relief. *Quaternary Research*, *1*(1), 103–120. https://doi.org/10.1016/0033-5894(70)90013-X

Dai, A., Zhao, T., & Chen, J. (2018). Climate change and drought: A precipitation and evaporation perspective. *Current Climate Change Reports*, *4*(3), 301–312. https://doi.org/10.1007/s40641-018-0101-6

Danabasoglu, G., Lamarque, J.-F., Bacmeister, J., Bailey, D. A., DuVivier, A. K., Edwards, J., et al. (2020). The Community Earth System Model Version 2 (CESM2). *Journal of Advances in Modeling Earth Systems*, *12*(2), e2019MS001916. https://doi.org/10.1029/2019MS001916

Dargie, G. C., Lawson, I. T., Rayden, T. J., Miles, L., Mitchard, E. T. A., Page, S. E., et al. (2019). Congo basin peatlands: Threats and conservation priorities. *Mitigation and Adaptation Strategies for Global Change*, *24*(4), 669–686. https://doi.org/10.1007/s11027-017-9774-8

Dargie, G. C., Lewis, S. L., Lawson, I. T., Mitchard, E. T. A., Page, S. E., Bocko, Y. E., & Ifo, S. A. (2017). Age, extent and carbon storage of the central Congo Basin peatland complex. *Nature*, *542*(7639), 86–90. https://doi.org/10.1038/nature21048

Davidson, N. C. (2014). How much wetland has the World lost? Long-Term and recent trends in global wetland area. *Marine and Freshwater Research*, *65*(10), 934. https://doi.org/10.1071/MF14173

Davidson, N. C., & Finlayson, C. M. (2018). Extent, regional distribution and changes in area of different classes of Wetland. *Marine and Freshwater Research*, *69*(10), 1525–1533. https://doi.org/10.1071/MF17377

Davidson, N. C., Fluet-Chouinard, E., & Finlayson, C. M. (2018). Global extent and distribution of wetlands: Trends and issues. *Marine and Freshwater Research*, *69*(4), 620–627. https://doi.org/10.1071/MF17019

Dean, J. F., Middelburg, J. J., Röckmann, T., Aerts, R., Blauw, L. G., Egger, M., et al. (2018). Methane feedbacks to the global climate system in a warmer world. *Reviews of Geophysics*, *56*(1), 207–250. https://doi.org/10.1002/2017RG000559

Decharme, B., Delire, C., Minvielle, M., Colin, J., Vergnes, J.-P., Alias, A., et al. (2019). Recent changes in the ISBA-CTRIP land surface system for use in the CNRM-CM6 climate model and in global off-line hydrological applications. *Journal of Advances in Modeling Earth Systems*, *11*(5), 1207–1252. https://doi.org/10.1029/2018MS001545

Decharme, B., & Douville, H. (2006). Introduction of a sub-grid hydrology in the ISBA land surface model. *Climate Dynamics*, *26*(1), 65–78. https://doi.org/10.1007/s00382-005-0059-7

Decharme, B., & Douville, H. (2007). Global validation of the ISBA sub-grid hydrology. *Climate Dynamics*, *29*(1), 21–37. https://doi.org/10.1007/s00382-006-0216-7

Decharme, B., Douville, H., Boone, A., Habets, F., & Noilhan, J. (2006). Impact of an exponential profile of saturated hydraulic conductivity within the ISBA LSM: Simulations over the Rhône Basin. *Journal of Hydrometeorology*, *7*(1), 61–80. https://doi.org/10.1175/JHM469.1

Delire, C., Séférian, R., Decharme, B., Alkama, R., Calvet, J.-C., Carrer, D., et al. (2020). The global land carbon cycle simulated with ISBA-CTRIP: Improvements over the last decade. *Journal of Advances in Modeling Earth Systems*, *12*(9), e2019MS001886. https://doi.org/10.1029/2019MS001886

Douville, H., Raghavan, K., Renwick, J., Allan, R. P., Arias, P. A., Barlow, M., et al. (2021). Water cycle changes. In V. P. Masson-Delmotte, P. Zhai, A. Pirani, S. L. Connors, C. Péan, S. Berger, et al. (Eds.), *Climate change 2021: The physical science basis. Contribution of working group I to 45 the sixth assessment report of the intergovernmental panel on climate change* (pp. 1055–1210). Cambridge University Press. Retrieved from https://centaur.reading.ac.uk/101319/

Dredge, L. A., & Dyke, L. D. (2020). Landscapes and landforms of the Hudson bay lowlands. In O. Slaymaker & N. Catto (Eds.), *Landscapes and landforms of eastern Canada* (pp. 211–227). Springer International Publishing. https://doi.org/10.1007/978-3-030-35137-3_8

Dunne, J. P., Horowitz, L. W., Adcroft, A. J., Ginoux, P., Held, I. M., John, J. G., et al. (2020). The GFDL Earth System Model version 4.1 (GFDL-ESM 4.1): Overall coupled model description and simulation characteristics. *Journal of Advances in Modeling Earth Systems*, *12*(11), e2019MS002015. https://doi.org/10.1029/2019MS002015

Eyring, V., Bony, S., Meehl, G. A., Senior, C. A., Stevens, B., Stouffer, R. J., & Taylor, K. E. (2016). Overview of the Coupled Model Intercomparison Project phase 6 (CMIP6) experimental design and organization. *Geoscientific Model Development*, *9*(5), 1937–1958. https://doi.org/10.5194/gmd-9-1937-2016

Famiglietti, J. S., & Wood, E. F. (1994). Multiscale modeling of spatially variable water and energy balance processes. *Water Resources Research*, *30*(11), 3061–3078. https://doi.org/10.1029/94WR01498

Farquharson, L. M., Romanovsky, V. E., Cable, W. L., Walker, D. A., Kokelj, S. V., & Nicolsky, D. (2019). Climate change drives widespread and rapid thermokarst development in very cold permafrost in the Canadian high Arctic. *Geophysical Research Letters*, *46*(12), 6681–6689. https://doi.org/10.1029/2019GL082187

Fluet-Chouinard, E., Stocker, B. D., Zhang, Z., Malhotra, A., Melton, J. R., Poulter, B., et al. (2023). Extensive global wetland loss over the past three centuries. *Nature*, *614*(7947), 281–286. https://doi.org/10.1038/s41586-022-05572-6

Garcin, Y., Schefuß, E., Dargie, G. C., Hawthorne, D., Lawson, I. T., Sebag, D., et al. (2022). Hydroclimatic vulnerability of peat carbon in the central Congo Basin. *Nature*, *612*(7939), 277–282. https://doi.org/10.1038/s41586-022-05389-3

Gardner, R. C., & Finlayson, M. (2018). *Global wetland outlook: State of the World's wetlands and their services to people 2018*. Secretariat of the Ramsar Convention.

Gedney, N., & Cox, P. M. (2003). The sensitivity of global climate model simulations to the representation of soil moisture heterogeneity. *Journal of Hydrometeorology*, *4*(6), 1265–1275. https://doi.org/10.1175/1525-7541(2003)004⟨1265:TSOGCM⟩2.0.CO;2

Gloor, M., Gatti, L. V., Wilson, C., Parker, R. J., Boesch, H., Popa, E., et al. (2021). Large methane emissions from the Pantanal during rising water-levels revealed by regularly measured lower troposphere CH4 profiles. *Global Biogeochemical Cycles*, *35*(10), e2021GB006964. https://doi.org/10.1029/2021GB006964

Grosse, G., Jones, B. M., & Arp, C. D. (2013). Thermokarst lakes, drainage, and drained basins. *Treatise on Geomorphology*, *8*, 325–353. https://doi.org/10.1016/B978-0-12-374739-6.00216-5

Gumbricht, T., Roman-Cuesta, R. M., Verchot, L., Herold, M., Wittmann, F., Householder, E., et al. (2017). An expert system model for mapping tropical wetlands and peatlands reveals South America as the largest contributor. *Global Change Biology*, *23*(9), 3581–3599. https://doi.org/10.1111/gcb.13689

Habets, F., & Saulnier, G. M. (2001). Subgrid runoff parameterization. *Physics and Chemistry of the Earth—Part B: Hydrology, Oceans and Atmosphere*, *26*(5), 455–459. https://doi.org/10.1016/S1464-1909(01)00034-X

Hardouin, L., Decharme, B., Colin, J., & Delire, C. (2024). Scripts and datas for "climate-driven projections of future global wetlands extent" (version v1) [Dataset, Software]. *Zenodo*. 11263132. https://doi.org/10.5281/zenodo.11263132

Harenda, K. M., Lamentowicz, M., Samson, M., & Chojnicki, B. H. (2018). The role of peatlands and their carbon storage function in the context of climate change. In *Interdisciplinary approaches for sustainable development goals* (pp. 169–187). Springer. https://doi.org/10.1007/978-3-319-71788-3_12

Harper, A. B., Cox, P. M., Friedlingstein, P., Wiltshire, A. J., Jones, C. D., Sitch, S., et al. (2016). Improved representation of plant functional types and physiology in the Joint UK Land Environment Simulator (JULES v4.2) using plant trait information. *Geoscientific Model Development*, *9*(7), 2415–2440. https://doi.org/10.5194/gmd-9-2415-2016

Harper, A. B., Wiltshire, A. J., Cox, P. M., Friedlingstein, P., Jones, C. D., Mercado, L. M., et al. (2018). Vegetation distribution and terrestrial carbon cycle in a carbon cycle configuration of JULES4.6 with new plant functional types. *Geoscientific Model Development*, *11*(7), 2857–2873. https://doi.org/10.5194/gmd-11-2857-2018

Huang, Y., Ciais, P., Luo, Y., Zhu, D., Wang, Y., Qiu, C., et al. (2021). Tradeoff of CO_2 and CH_4 emissions from global peatlands under water-table drawdown. *Nature Climate Change*, *11*(7), 618–622. https://doi.org/10.1038/s41558-021-01059-w

Hugelius, G., Loisel, J., Chadburn, S., Jackson, R. B., Jones, M., MacDonald, G., et al. (2020). Large stocks of peatland carbon and nitrogen are vulnerable to permafrost thaw. *Proceedings of the National Academy of Sciences*, *117*(34), 20438–20446. https://doi.org/10.1073/pnas.1916387117

Hugelius, G., Strauss, J., Zubrzycki, S., Harden, J. W., Schuur, E. a. G., Ping, C.-L., et al. (2014). Estimated stocks of circumpolar permafrost carbon with quantified uncertainty ranges and identified data gaps. *Biogeosciences*, *11*(23), 6573–6593. https://doi.org/10.5194/bg-11-6573-2014

Hurtt, G. C., Chini, L., Sahajpal, R., Frolking, S., Bodirsky, B. L., Calvin, K., et al. (2020). Harmonization of global land use change and management for the period 850–2100 (LUH2) for CMIP6. *Geoscientific Model Development*, *13*(11), 5425–5464. https://doi.org/10.5194/gmd-13-5425-2020

Ikeda-Castrillon, S. K., Oliveira-Junior, E. S., Rossetto, O. C., Saito, C. H., & Wantzen, K. M. (2020). The Pantanal: A seasonal Neotropical wetland under threat. In *The Palgrave handbook of global sustainability* (pp. 1–27). Springer International Publishing. https://doi.org/10.1007/978-3-030-38948-2_36-1

Junk, W. J., & Cunha, C. N. D. (2005). Pantanal: A large South American wetland at a crossroads. *Ecological Engineering*, *24*(4), 391–401. https://doi.org/10.1016/j.ecoleng.2004.11.012

Junk, W. J., Piedade, M. T. F., Schöngart, J., Cohn-Haft, M., Adeney, J. M., & Wittmann, F. (2011). A classification of major naturally-occurring Amazonian lowland wetlands. *Wetlands*, *31*(4), 623–640. https://doi.org/10.1007/s13157-011-0190-7

Karam, S., Seidou, O., Nagabhatla, N., Perera, D., & Tshimanga, R. M. (2022). Assessing the impacts of climate change on climatic extremes in the Congo River Basin. *Climatic Change*, *170*(3), 40. https://doi.org/10.1007/s10584-022-03326-x

Karlsson, J., Serikova, S., Vorobyev, S. N., Rocher-Ros, G., Denfeld, B., & Pokrovsky, O. S. (2021). Carbon emission from Western Siberian inland waters. *Nature Communications*, *12*(1), 825. https://doi.org/10.1038/s41467-021-21054-1

Keddy, P. A., Fraser, L. H., Solomeshch, A. I., Junk, W. J., Campbell, D. R., Arroyo, M. T. K., & Alho, C. J. R. (2009). Wet and wonderful: The world's largest wetlands are conservation priorities. *BioScience*, *59*(1), 39–51. https://doi.org/10.1525/bio.2009.59.1.8

Kirschke, S., Bousquet, P., Ciais, P., Saunois, M., Canadell, J. G., Dlugokencky, E. J., et al. (2013). Three decades of global methane sources and sinks. *Nature Geoscience*, *6*(10), 813–823. https://doi.org/10.1038/ngeo1955

Kleinen, T., Brovkin, V., & Schuldt, R. J. (2012). A dynamic model of wetland extent and peat accumulation: Results for the Holocene. *Biogeosciences*, *9*(1), 235–248. https://doi.org/10.5194/bg-9-235-2012

Kokelj, S. V., & Jorgenson, M. T. (2013). Advances in thermokarst research. *Permafrost and Periglacial Processes*, *24*(2), 108–119. https://doi.org/10.1002/ppp.1779

Koster, R. D., Suarez, M. J., Ducharne, A., Stieglitz, M., & Kumar, P. (2000). A catchment-based approach to modeling land surface processes in a general circulation model: 1. Model structure. *Journal of Geophysical Research*, *105*(D20), 24809–24822. https://doi.org/10.1029/2000JD900327

Koven, C. D., Riley, W. J., & Stern, A. (2013). Analysis of permafrost thermal dynamics and response to climate change in the CMIP5 Earth system models. *Journal of Climate*, *26*(6), 1877–1900. https://doi.org/10.1175/JCLI-D-12-00228.1

Kowalczyk, E. A., Stevens, L. E., Law, R. M., Harman, I. N., Dix, M., Franklin, C. N., & Wang, Y.-P. (2016). The impact of changing the land surface scheme in ACCESS (v1.0/1.1) on the surface climatology. *Geoscientific Model Development*, *9*(8), 2771–2791. https://doi.org/10.5194/gmd-9-2771-2016

Kowalczyk, E. A., Wang, Y. P., Law, R. M., Davies, H. L., McGregor, J. L., & Abramowitz, G. (2006). The CSIRO Atmosphere Biosphere Land Exchange (CABLE) model for use in climate models and as an offline model.

Kremenetski, K. V., Velichko, A. A., Borisova, O. K., MacDonald, G. M., Smith, L. C., Frey, K. E., & Orlova, L. A. (2003). Peatlands of the western Siberian lowlands: Current knowledge on zonation, carbon content and late quaternary history. *Quaternary Science Reviews*, *22*(5), 703–723. https://doi.org/10.1016/S0277-3791(02)00196-8

Kreplin, H. N., Santos Ferreira, C. S., Destouni, G., Keesstra, S. D., Salvati, L., & Kalantari, Z. (2021). Arctic wetland system dynamics under climate warming. *WIREs Water*, *8*(4), e1526. https://doi.org/10.1002/wat2.1526

Krinner, G. (2003). Impact of lakes and wetlands on boreal climate. *Journal of Geophysical Research*, *108*(D16), 4520. https://doi.org/10.1029/2002JD002597

Krinner, G., Viovy, N., de Noblet-Ducoudré, N., Ogée, J., Polcher, J., Friedlingstein, P., et al. (2005). A dynamic global vegetation model for studies of the coupled atmosphere-biosphere system. *Global Biogeochemical Cycles*, *19*(1). https://doi.org/10.1029/2003GB002199

Lawrence, D. M., Fisher, R. A., Koven, C. D., Oleson, K. W., Swenson, S. C., Bonan, G., et al. (2019). The community land model version 5: Description of new features, benchmarking, and impact of forcing uncertainty. *Journal of Advances in Modeling Earth Systems*, *11*(12), 4245–4287. https://doi.org/10.1029/2018MS001583

Lázaro, W. L., Oliveira-Júnior, E. S., Silva, C. J. d., Castrillon, S. K. I., & Muniz, C. C. (2020). Climate change reflected in one of the largest wetlands in the world: An overview of the northern Pantanal water regime. *Acta Limnologica Brasiliensia*, *32*, e104. https://doi.org/10.1590/s2179-975x7619

Lee, H., Beighley, R. E., Alsdorf, D., Jung, H. C., Shum, C. K., Duan, J., et al. (2011). Characterization of terrestrial water dynamics in the Congo Basin using GRACE and satellite radar altimetry. *Remote Sensing of Environment*, *115*(12), 3530–3538. https://doi.org/10.1016/j.rse.2011.08.015

Lee, H., Yuan, T., Jung, H. C., & Beighley, E. (2015). Mapping wetland water depths over the central Congo Basin using PALSAR ScanSAR, Envisat altimetry, and MODIS VCF data. *Remote Sensing of Environment*, *159*, 70–79. https://doi.org/10.1016/j.rse.2014.11.030

Lehner, B., & Döll, P. (2004). Development and validation of a global database of lakes, reservoirs and wetlands. *Journal of Hydrology*, *296*(1), 1–22. https://doi.org/10.1016/j.jhydrol.2004.03.028

Lehner, B., Verdin, K., & Jarvis, A. (2008). New global hydrography derived from spaceborne elevation data. *Eos, Transactions American Geophysical Union*, *89*(10), 93–94. https://doi.org/10.1029/2008EO100001

Li, W., Zhang, Y., Shi, X., Zhou, W., Huang, A., Mu, M., et al. (2019). Development of land surface model BCC_avim2.0 and its preliminary performance in ls3mip/CMIP6. *Journal of Meteorological Research*, *33*(5), 851–869. https://doi.org/10.1007/s13351-019-9016-y

Loisel, J., van Bellen, S., Pelletier, L., Talbot, J., Hugelius, G., Karran, D., et al. (2017). Insights and issues with estimating Northern Peatland carbon stocks and fluxes since the Last Glacial Maximum. *Earth-Science Reviews*, *165*, 59–80. https://doi.org/10.1016/j.earscirev.2016.12.001

Loisel, J., Yu, Z., Beilman, D. W., Camill, P., Alm, J., Amesbury, M. J., et al. (2014). A database and synthesis of northern peatland soil properties and Holocene carbon and nitrogen accumulation. *The Holocene*, *24*(9), 1028–1042. https://doi.org/10.1177/0959683614538073

Lovato, T., Peano, D., Butenschön, M., Materia, S., Iovino, D., Scoccimarro, E., et al. (2022). CMIP6 simulations with the CMCC Earth System Model (CMCC-ESM2). *Journal of Advances in Modeling Earth Systems*, *14*(3), e2021MS002814. https://doi.org/10.1029/2021MS002814

Mamet, S. D., Chun, K. P., Kershaw, G. G. L., Loranty, M. M., & Peter Kershaw, G. (2017). Recent increases in permafrost thaw rates and areal loss of Palsas in the western northwest territories, Canada. *Permafrost and Periglacial Processes*, *28*(4), 619–633. https://doi.org/10.1002/ppp.1951

Mankin, J. S., Seager, R., Smerdon, J. E., Cook, B. I., & Williams, A. P. (2019). Mid-latitude freshwater availability reduced by projected vegetation responses to climate change. *Nature Geoscience*, *12*(12), 983–988. https://doi.org/10.1038/s41561-019-0480-x

Marengo, J. A. (2004). Interdecadal variability and trends of rainfall across the Amazon basin. *Theoretical and Applied Climatology*, *78*(1), 79–96. https://doi.org/10.1007/s00704-004-0045-8

Marengo, J. A., Cunha, A. P., Cuartas, L. A., Deusdará Leal, K. R., Broedel, E., Seluchi, M. E., et al. (2021). Extreme drought in the Brazilian Pantanal in 2019–2020: Characterization, causes, and impacts. *Frontiers in Water*, *3*, 639204. https://doi.org/10.3389/frwa.2021.639204

Marengo, J. A., & Espinoza, J. C. (2016). Extreme seasonal droughts and floods in Amazonia: Causes, trends and impacts. *International Journal of Climatology*, *36*(3), 1033–1050. https://doi.org/10.1002/joc.4420

Marengo, J. A., Oliveira, G. S., & Alves, L. M. (2016). Climate change scenarios in the Pantanal. In I. Bergier & M. L. Assine (Eds.), *Dynamics of the Pantanal wetland in SouthSouth America* (pp. 227–238). Springer International Publishing. https://doi.org/10.1007/698_2015_357

Marthews, T. R., Dadson, S. J., Lehner, B., Abele, S., & Gedney, N. (2015a). High-resolution global topographic index values [Dataset]. *NERC Environmental Information Data Centre*. https://doi.org/10.5285/6b0c4358-2bf3-4924-aa8f-793d468b92be

Marthews, T. R., Dadson, S. J., Lehner, B., Abele, S., & Gedney, N. (2015b). High-resolution global topographic index values for use in large-scale hydrological modelling. *Hydrology and Earth System Sciences*, *19*(1), 91–104. https://doi.org/10.5194/hess-19-91-2015

Masson-Delmotte, V., Zhai, P., Pirani, A., Connors, S. L., Péan, C., Chen, Y., et al. (2021). Working group I contribution to the sixth assessment report of the intergovernmental panel on climate change.

Meinshausen, M., Vogel, E., Nauels, A., Lorbacher, K., Meinshausen, N., Etheridge, D. M., et al. (2017). Historical greenhouse gas concentrations for climate modelling (CMIP6). *Geoscientific Model Development*, *10*(5), 2057–2116. https://doi.org/10.5194/gmd-10-2057-2017

Melack, J. M., & Hess, L. L. (2011). Remote sensing of the distribution and extent of wetlands in the Amazon Basin. In W. J. Junk, M. T. F. Piedade, F. Wittmann, J. Schöngart, & P. Parolin (Eds.), *Amazonian floodplain forests: Ecophysiology, biodiversity and sustainable management* (pp. 43–59). Springer. https://doi.org/10.1007/978-90-481-8725-6_3

Melton, J. R., Chan, E., Millard, K., Fortier, M., Winton, R. S., Martín-López, J. M., et al. (2022). A map of global peatland extent created using Machine Learning (Peat-ML). *Geoscientific Model Development*, *15*(12), 4709–4738. https://doi.org/10.5194/gmd-15-4709-2022

Milly, P. C. D., & Dunne, K. A. (2016). Potential evapotranspiration and continental drying. *Nature Climate Change*, *6*(10), 946–949. https://doi.org/10.1038/nclimate3046

Mitra, S., Wassmann, R., & Vlek, P. L. G. (2005). An appraisal of global wetland area and its organic carbon stock. *Current Science*, *88*(1), 25–35. Retrieved from https://www.jstor.org/stable/24110090

Mitsch, W. J., Nahlik, A., Wolski, P., Bernal, B., Zhang, L., & Ramberg, L. (2010). Tropical wetlands: Seasonal hydrologic pulsing, carbon sequestration, and methane emissions. *Wetlands Ecology and Management*, *18*(5), 573–586. https://doi.org/10.1007/s11273-009-9164-4

Niu, G.-Y., Yang, Z.-L., Dickinson, R. E., & Gulden, L. E. (2005). A simple TOPMODEL-based runoff parameterization (SIMTOP) for use in global climate models. *Journal of Geophysical Research*, *110*(D21), D21106. https://doi.org/10.1029/2005JD006111

Nunes da Cunha, C., & Junk, W. (2004). Year-to-year changes in water level drive the invasion of Vochysia divergens in Pantanal grasslands. *Applied Vegetation Science*, *7*(1), 103–110. https://doi.org/10.1111/j.1654-109X.2004.tb00600.x

Olefeldt, D., Euskirchen, E. S., Harden, J., Kane, E., McGuire, A. D., Waldrop, M. P., & Turetsky, M. R. (2017). A decade of boreal rich fen greenhouse gas fluxes in response to natural and experimental water table variability. *Global Change Biology*, *23*(6), 2428–2440. https://doi.org/10.1111/gcb.13612

Oleson, K., Lawrence, M., Bonan, B., Drewniak, B., Huang, M., Koven, D., et al. (2013). Technical description of version 4.5 of the Community Land Model (CLM). https://doi.org/10.5065/D6RR1W7M

Oleson, W., Lawrence, M., Bonan, B., Flanner, G., Kluzek, E., Lawrence, J., et al. (2010). Technical description of version 4.0 of the Community Land Model (CLM). https://doi.org/10.5065/D6FB50WZ

Olivares, I., Svenning, J.-C., van Bodegom, P. M., & Balslev, H. (2015). Effects of warming and drought on the vegetation and plant diversity in the Amazon Basin. *The Botanical Review*, *81*(1), 42–69. https://doi.org/10.1007/s12229-014-9149-8

Olthof, I., & Fraser, R. H. (2024). Mapping surface water dynamics (1985–2021) in the Hudson Bay Lowlands, Canada using sub-pixel Landsat analysis. *Remote Sensing of Environment*, *300*, 113895. https://doi.org/10.1016/j.rse.2023.113895

O'Neill, B. C., Kriegler, E., Ebi, K. L., Kemp-Benedict, E., Riahi, K., Rothman, D. S., et al. (2017). The roads ahead: Narratives for shared socioeconomic pathways describing world futures in the 21st century. *Global Environmental Change*, *42*, 169–180. https://doi.org/10.1016/j.gloenvcha.2015.01.004

O'Neill, B. C., Tebaldi, C., van Vuuren, D. P., Eyring, V., Friedlingstein, P., Hurtt, G., et al. (2016). The scenario Model Intercomparison Project (ScenarioMIP) for CMIP6. *Geoscientific Model Development*, *9*(9), 3461–3482. https://doi.org/10.5194/gmd-9-3461-2016

Osterkamp, T. E., Viereck, L., Shur, Y., Jorgenson, M. T., Racine, C., Doyle, A., & Boone, R. D. (2000). Observations of Thermokarst and Its Impact on Boreal Forests in Alaska, U.S.A. *Arctic Antarctic and Alpine Research*, *32*(3), 303–315. https://doi.org/10.1080/15230430.2000.12003368

Parsons, L. A. (2020). Implications of CMIP6 Projected Drying Trends for 21st Century Amazonian Drought Risk. *Earth's Future*, *8*(10), e2020EF001608. https://doi.org/10.1029/2020EF001608

Peng, S., Lin, X., Thompson, R. L., Xi, Y., Liu, G., Hauglustaine, D., et al. (2022). Wetland emission and atmospheric sink changes explain methane growth in 2020. *Nature*, *612*(7940), 477–482. https://doi.org/10.1038/s41586-022-05447-w

Poggio, L., de Sousa, L. M., Batjes, N. H., Heuvelink, G. B. M., Kempen, B., Ribeiro, E., & Rossiter, D. (2021). SoilGrids 2.0: Producing soil information for the globe with quantified spatial uncertainty. *SOIL*, *7*(1), 217–240. https://doi.org/10.5194/soil-7-217-2021

Polishchuk, Y. M., Bogdanov, A. N., Muratov, I. N., Polishchuk, V. Y., Lim, A., Manasypov, R. M., et al. (2018). Minor contribution of small thaw ponds to the pools of carbon and methane in the inland waters of the permafrost-affected part of the Western Siberian Lowland. *Environmental Research Letters*, *13*(4), 045002. https://doi.org/10.1088/1748-9326/aab046

Pott, A., Oliveira, A. K. M., Damasceno-Junior, G. A., & Silva, J. S. V. (2011). Plant diversity of the Pantanal Wetland. *Brazilian Journal of Biology*, *71*(1), 265–273. https://doi.org/10.1590/S1519-69842011000200005

Quinton, W., Hayashi, M., & Chasmer, L. (2011). Permafrost-thaw-induced land-cover change in the Canadian subarctic: Implications for water resources. *Hydrological Processes*, *25*(1), 152–158. https://doi.org/10.1002/hyp.7894

Rennermalm, A. K., Wood, E. F., & Troy, T. J. (2010). Observed changes in pan-arctic cold-season minimum monthly river discharge. *Climate Dynamics*, *35*(6), 923–939. https://doi.org/10.1007/s00382-009-0730-5

Riahi, K., van Vuuren, D. P., Kriegler, E., Edmonds, J., O'Neill, B. C., Fujimori, S., et al. (2017). The Shared Socioeconomic Pathways and their energy, land use, and greenhouse gas emissions implications: An overview. *Global Environmental Change*, *42*, 153–168. https://doi.org/10.1016/j.gloenvcha.2016.05.009

Ringeval, B., Decharme, B., Piao, S. L., Ciais, P., Papa, F., de Noblet-Ducoudré, N., et al. (2012). Modelling sub-grid wetland in the ORCHIDEE global land surface model: Evaluation against river discharges and remotely sensed data. *Geoscientific Model Development*, *5*(4), 941–962. https://doi.org/10.5194/gmd-5-941-2012

Ringeval, B., de Noblet-Ducoudré, N., Ciais, P., Bousquet, P., Prigent, C., Papa, F., & Rossow, W. B. (2010). An attempt to quantify the impact of changes in wetland extent on methane emissions on the seasonal and interannual time scales. *Global Biogeochemical Cycles*, *24*(2), GB2003. https://doi.org/10.1029/2008GB003354

Rodell, M., Houser, P. R., Jambor, U., Gottschalck, J., Mitchell, K., Meng, C.-J., et al. (2004). The Global Land Data Assimilation System. *Bulletin of the American Meteorological Society*, *85*(3), 381–394. https://doi.org/10.1175/BAMS-85-3-381

Roucoux, K., Lawson, I., Baker, T., Del Castillo Torres, D., Draper, F., Lähteenoja, O., et al. (2017). Threats to intact tropical peatlands and opportunities for their conservation. *Conservation Biology*, *31*(6), 1283–1292. https://doi.org/10.1111/cobi.12925

Rouse, W. R. (1991). Impacts of Hudson Bay on the Terrestrial Climate of the Hudson Bay Lowlands*. *Arctic and Alpine Research*, *23*(1), 24–30. https://doi.org/10.1080/00040851.1991.12002815

Rowland, J. C., Jones, C. E., Altmann, G., Bryan, R., Crosby, B. T., Hinzman, L. D., et al. (2010). Arctic Landscapes in Transition: Responses to Thawing Permafrost. *Eos, Transactions American Geophysical Union*, *91*(26), 229–230. https://doi.org/10.1029/2010EO260001

Saulnier, G.-M., & Datin, R. (2004). Analytical solution to a bias in the TOPMODEL framework balance. *Hydrological Processes*, *18*(7), 1195–1218. https://doi.org/10.1002/hyp.1346

Saunders, D., & Kalff, J. (2001). Nitrogen retention in wetlands, lakes and rivers. *Hydrobiologia*, *443*(1), 205–212. https://doi.org/10.1023/A:1017506914063

Saunois, M., Stavert, A. R., Poulter, B., Bousquet, P., Canadell, J. G., Jackson, R. B., et al. (2020). The Global Methane Budget 2000–2017. *Earth System Science Data*, *12*(3), 1561–1623. https://doi.org/10.5194/essd-12-1561-2020

Schroeder, R., McDonald, K. C., Chapman, B. D., Jensen, K., Podest, E., Tessler, Z. D., et al. (2015). Development and Evaluation of a Multi-Year Fractional Surface Water Data Set Derived from Active/Passive Microwave Remote Sensing Data. *Remote Sensing*, *7*(12), 16688–16732. https://doi.org/10.3390/rs71215843

Séférian, R., Nabat, P., Michou, M., Saint-Martin, D., Voldoire, A., Colin, J., et al. (2019). Evaluation of CNRM Earth System Model, CNRM-ESM2-1: Role of Earth System Processes in Present-Day and Future Climate. *Journal of Advances in Modeling Earth Systems*, *11*(12), 4182–4227. https://doi.org/10.1029/2019MS001791

Seland, y., Bentsen, M., Olivié, D., Toniazzo, T., Gjermundsen, A., Graff, L. S., et al. (2020). Overview of the Norwegian Earth System Model (NorESM2) and key climate response of CMIP6 DECK, historical, and scenario simulations. *Geoscientific Model Development*, *13*(12), 6165–6200. https://doi.org/10.5194/gmd-13-6165-2020

Sellar, A. A., Jones, C. G., Mulcahy, J. P., Tang, Y., Yool, A., Wiltshire, A., et al. (2019). UKESM1: Description and Evaluation of the U.K. Earth System Model. *Journal of Advances in Modeling Earth Systems*, *11*(12), 4513–4558. https://doi.org/10.1029/2019MS001739

Sheng, Y., Smith, L. C., MacDonald, G. M., Kremenetski, K. V., Frey, K. E., Velichko, A. A., et al. (2004). A high-resolution GIS-based inventory of the west Siberian peat carbon pool. *Global Biogeochemical Cycles*, *18*(3), GB3004. https://doi.org/10.1029/2003GB002190

Sivapalan, M., Beven, K., & Wood, E. F. (1987). On hydrologic similarity: 2. A scaled model of storm runoff production. *Water Resources Research*, *23*(12), 2266–2278. https://doi.org/10.1029/WR023i012p02266

Smith, L. C., Pavelsky, T. M., MacDonald, G. M., Shiklomanov, A. I., & Lammers, R. B. (2007). Rising minimum daily flows in Northern Eurasian rivers: A growing influence of groundwater in the high-latitude hydrologic cycle. *Journal of Geophysical Research*, *112*(G4), G04S47. https://doi.org/10.1029/2006JG000327

Smith, L. C., Sheng, Y., MacDonald, G. M., & Hinzman, L. D. (2005). Disappearing Arctic Lakes. *Science*, *308*(5727), 1429. https://doi.org/10.1126/science.1108142

Sothe, C., Gonsamo, A., Arabian, J., Kurz, W. A., Finkelstein, S. A., & Snider, J. (2022). Large Soil Carbon Storage in Terrestrial Ecosystems of Canada. *Global Biogeochemical Cycles*, *36*(2), e2021GB007213. https://doi.org/10.1029/2021GB007213

Sterling, S. M., Ducharne, A., & Polcher, J. (2013). The impact of global land-cover change on the terrestrial water cycle. *Nature Climate Change*, *3*(4), 385–390. https://doi.org/10.1038/nclimate1690

Stieglitz, M., Rind, D., Famiglietti, J., & Rosenzweig, C. (1997). An Efficient Approach to Modeling the Topographic Control of Surface Hydrology for Regional and Global Climate Modeling. *Journal of Climate*, *10*(1), 118–137. https://doi.org/10.1175/1520-0442(1997)010⟨0118:AEATMT⟩2.0.CO;2

Stocker, B. D., Spahni, R., & Joos, F. (2014). Dyptop: A cost-efficient TOPMODEL implementation to simulate sub-grid spatio-temporal dynamics of global wetlands and peatlands. *Geoscientific Model Development*, *7*(6), 3089–3110. https://doi.org/10.5194/gmd-7-3089-2014

Swart, N. C., Cole, J. N. S., Kharin, V. V., Lazare, M., Scinocca, J. F., Gillett, N. P., et al. (2019). The Canadian Earth System Model version 5 (CanESM5.0.3). *Geoscientific Model Development*, *12*(11), 4823–4873. https://doi.org/10.5194/gmd-12-4823-2019

Taylor, K. E., Stouffer, R. J., & Meehl, G. A. (2012). An Overview of CMIP5 and the Experiment Design. *Bulletin of the American Meteorological Society*, *93*(4), 485–498. https://doi.org/10.1175/BAMS-D-11-00094.1

Voigt, C., Marushchak, M. E., Mastepanov, M., Lamprecht, R. E., Christensen, T. R., Dorodnikov, M., et al. (2019). Ecosystem carbon response of an Arctic peatland to simulated permafrost thaw. *Global Change Biology*, *25*(5), 1746–1764. https://doi.org/10.1111/gcb.14574

Voldoire, A., Saint-Martin, D., Sénési, S., Decharme, B., Alias, A., Chevallier, M., et al. (2019). Evaluation of CMIP6 DECK Experiments With CNRM-CM6-1. *Journal of Advances in Modeling Earth Systems*, *11*(7), 2177–2213. https://doi.org/10.1029/2019MS001683

Walter, B. P., & Heimann, M. (2000). A process-based, climate-sensitive model to derive methane emissions from natural wetlands: Application to five wetland sites, sensitivity to model parameters, and climate. *Global Biogeochemical Cycles*, *14*(3), 745–765. https://doi.org/10.1029/1999GB001204

Walvoord, M. A., & Striegl, R. G. (2007). Increased groundwater to stream discharge from permafrost thawing in the Yukon River basin: Potential impacts on lateral export of carbon and nitrogen. *Geophysical Research Letters*, *34*(12), L12402. https://doi.org/10.1029/2007GL030216

Wang, Y.-C., Hsu, H.-H., Chen, C.-A., Tseng, W.-L., Hsu, P.-C., Lin, C.-W., et al. (2021). Performance of the Taiwan Earth System Model in Simulating Climate Variability Compared With Observations and CMIP6 Model Simulations. *Journal of Advances in Modeling Earth Systems*, *13*(7), e2020MS002353. https://doi.org/10.1029/2020MS002353

Webb, E. E., & Liljedahl, A. K. (2023). Diminishing lake area across the northern permafrost zone. *Nature Geoscience*, *16*(3), 202–209. https://doi.org/10.1038/s41561-023-01128-z

Winden, J. F. v., Reichart, G.-J., McNamara, N. P., Benthien, A., & Damsté, J. S. S. (2012). Temperature-Induced Increase in Methane Release from Peat Bogs: A Mesocosm Experiment. *PLoS One*, *7*(6), e39614. https://doi.org/10.1371/journal.pone.0039614

Woo, M.-k., & Young, K. L. (2006). High Arctic wetlands: Their occurrence, hydrological characteristics and sustainability. *Journal of Hydrology*, *320*(3), 432–450. https://doi.org/10.1016/j.jhydrol.2005.07.025

Wu, T., Lu, Y., Fang, Y., Xin, X., Li, L., Li, W., et al. (2019). The Beijing Climate Center Climate System Model (BCC-CSM): The main progress from CMIP5 to CMIP6. *Geoscientific Model Development*, *12*(4), 1573–1600. https://doi.org/10.5194/gmd-12-1573-2019

Xi, Y., Peng, S., Ciais, P., & Chen, Y. (2021). Future impacts of climate change on inland Ramsar wetlands. *Nature Climate Change*, *11*(1), 45–51. https://doi.org/10.1038/s41558-020-00942-2

Xi, Y., Peng, S., Ducharne, A., Ciais, P., Gumbricht, T., Jimenez, C., et al. (2022). Gridded maps of wetlands dynamics over mid-low latitudes for 1980–2020 based on TOPMODEL. *Scientific Data*, *9*(1), 347. https://doi.org/10.1038/s41597-022-01460-w

Yvon-Durocher, G., Allen, A. P., Bastviken, D., Conrad, R., Gudasz, C., St-Pierre, A., et al. (2014). Methane fluxes show consistent temperature dependence across microbial to ecosystem scales. *Nature*, *507*(7493), 488–491. https://doi.org/10.1038/nature13164

Zakharova, E. A., Kouraev, A. V., Rémy, F., Zemtsov, V. A., & Kirpotin, S. N. (2014). Seasonal variability of the Western Siberia wetlands from satellite radar altimetry. *Journal of Hydrology*, *512*, 366–378. https://doi.org/10.1016/j.jhydrol.2014.03.002

Zedler, J. B., & Kercher, S. (2005). Wetland Resources: Status, Trends, Ecosystem Services, and Restorability. *Annual Review of Environment and Resources*, *30*(1), 39–74. https://doi.org/10.1146/annurev.energy.30.050504.144248

Zhang, Z., Fluet-Chouinard, E., Jensen, K., McDonald, K., Hugelius, G., Gumbricht, T., et al. (2021a). Development of the global dataset of Wetland Area and Dynamics for Methane Modeling (WAD2M). *Earth System Science Data*, *13*(5), 2001–2023. https://doi.org/10.5194/essd-13-2001-2021

Zhang, Z., Fluet-Chouinard, E., Jensen, K., McDonald, K., Hugelius, G., Gumbricht, T., et al. (2021b). Development of the global dataset of Wetland Area and Dynamics for Methane Modeling (WAD2M) (2.0) [Dataset]. *Zenodo*. https://doi.org/10.5281/zenodo.5553187

Zhang, Z., Poulter, B., Feldman, A. F., Ying, Q., Ciais, P., Peng, S., & Li, X. (2023). Recent intensification of wetland methane feedback. *Nature Climate Change*, *13*(5), 430–433. https://doi.org/10.1038/s41558-023-01629-0

Zhang, Z., Zimmermann, N. E., Kaplan, J. O., & Poulter, B. (2016). Modeling spatiotemporal dynamics of global wetlands: Comprehensive evaluation of a new sub-grid TOPMODEL parameterization and uncertainties. *Biogeosciences*, *13*(5), 1387–1408. https://doi.org/10.5194/bg-13-1387-2016

Zhao, B., & Zhuang, Q. (2023). Peatlands and their carbon dynamics in northern high latitudes from 1990 to 2300: A process-based biogeochemistry model analysis. *Biogeosciences*, *20*(1), 251–270. https://doi.org/10.5194/bg-20-251-2023

Zhao, M., Golaz, J.-C., Held, I. M., Guo, H., Balaji, V., Benson, R., et al. (2018). The GFDL Global Atmosphere and Land Model AM4.0/LM4.0: 2. Model Description, Sensitivity Studies, and Tuning Strategies. *Journal of Advances in Modeling Earth Systems*, *10*(3), 735–769. https://doi.org/10.1002/2017MS001209

Ziehn, T., Chamberlain, M. A., Law, R. M., Lenton, A., Bodman, R. W., Dix, M., et al. (2020). The Australian Earth System Model: ACCESS-ESM1.5. *Journal of Southern Hemisphere Earth Systems Science*, *70*(1), 193–214. https://doi.org/10.1071/ES19035

Zomer, R. J., Xu, J., & Trabucco, A. (2019). Global Aridity Index and Potential Evapotranspiration ET0 Database: Version 3 [Dataset]. *Scientific Data*, *9*(1), 409. https://doi.org/10.6084/m9.figshare.7504448.v6

Zomer, R. J., Xu, J., & Trabucco, A. (2022). Version 3 of the Global Aridity Index and Potential Evapotranspiration Database. *Scientific Data*, *9*(1), 409. https://doi.org/10.1038/s41597-022-01493-1